CONSTRAINING THE TIMING AND DEPOSITIONAL CONDITIONS OF THE MAIKOP FORMATION WITHIN THE KURA BASIN, EASTERN AZERBAIJAN,THROUGH THE APPLICATION OF RE-OS GEOCHRONOLOGY AND CHEMOSTRATIGRAPHY

A.M.Washburn[1], S. M. Hudson[1], D. Selby[2,4], N.Abdullayev[3] and N. Shiyanova[3]
[1]Department of Geological Sciences, Brigham Young University, Provo, UT 84602, USA.
[2]Department of Earth Sciences, Durham University, Durham DH1, UK.
[3]BP Azerbaijan, Baku,Azerbaijan.
[4] School of Earth Resources, China University of Geosciences,Wuhan, 430074 China.

Abstract

The Oligocene – Miocene Maikop Formation is the key source rock in the South Caspian and Kura Basins. The Maikop is composed of a thick (up to 3 km) succession of clay-rich mudstones containing up to 15% total organic carbon (TOC). Despite decades of study, the mudstones often lack precise age control – Maikop strata rarely contain diagnostic microfaunal assemblages which can be used for dating, stratigraphic correlation, or constraining the depositional setting. Using rhenium-osmium geochronology, this study adds important numerical age data for the Maikop Formation. Of five sample suites analyzed from the Kura Basin, eastern Azerbaijan, one Re-Os data-set produced a significant range in 187Re/188Os versus 187Os/188Os space to yield an isochron of 17.2 ± 3.2 Ma (Early Miocene). Other sample suites yielded imprecise Re-Os age constraints as a result of variable initial 187Os/188Os values and a limited range in 187Re/188Os versus 187Os/188Os space. The initial 187Os/188Os values of these data-sets were compared with the known 187Os/188Os values of seawater for the past 70 Ma to provide more qualitative age constraints. Pre-Maikopian strata from the Perikeshkul locality were found to coincide in 187Os/188Os values with an isotope excursion at the Eocene – Oligocene Transition (EOT), therefore indicating that deposition of Maikopian strata began around the EOT. While values such as this match well with global values, there are several 187Os/188Os values that are not easily explained by global ratios. Intervals with initial 187Os/188Os values that deviate significantly from global 187Os/188Os values suggest periodic basin restriction and the development of anoxia at discrete times as the basin transitioned towards a closed system. High Os abundances outside of expected global values are often coupled with enrichment in detrital elements (Al,Ti, Ga, Sc and La) and changes in basin circulation, suggesting changing basinal conditions and sediment routing dynamics related to the initial uplift of the Greater Caucasus Mountains, changes in sediment provenance, or changing proximity to the sediment source. Through generation of isochron age dates and imprecise Re-Os age constraints from the Maikop Formation, we gain a better understanding of the timing and nature of the evolution of the South Caspian Basin during this critical time period. Better age constrains will also help to better constrain the wealth of geochemical information already gathered within this petroleum-rich basin.

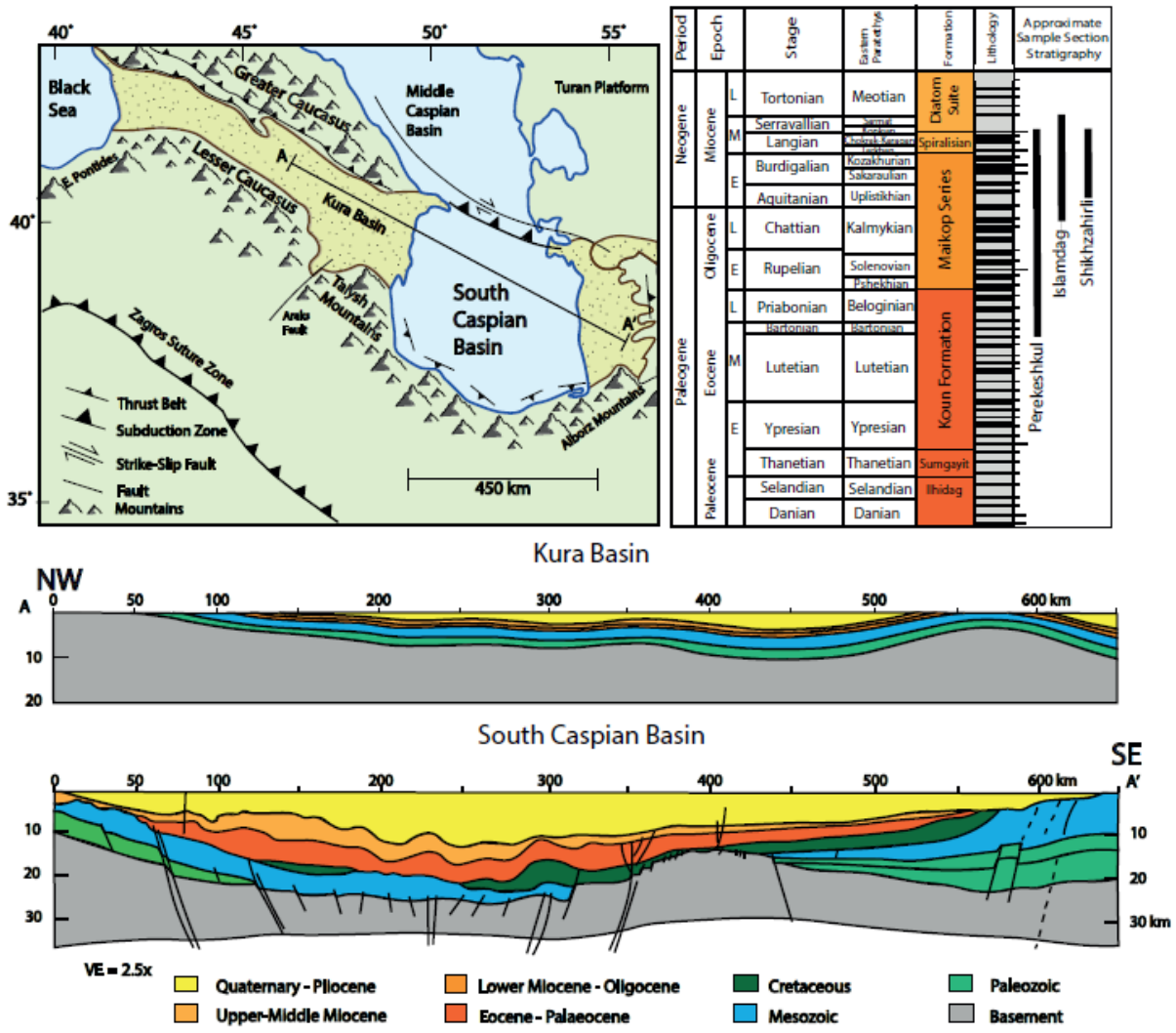

Fig. 1. Structural cartoon of the present-day South Caspian and Kura Basin areas with a generalised stratigraphic column, including the stratigraphic columns from this study (modified from Hudson *et al.*, 2016; and Brunet *et al.*, 2003). Cross section A-A' is divided into two parts: the South Caspian and Kura Basins. Note the great thickness of Pliocene to Quaternary sediments in the South Caspian Basin, indicating rapid deposition which has resulted in overpressuring.

INTRODUCTION

Understanding the evolution of the Paratethys is critical in resolving the formation of petroleum systems elements in sedimentary basins including the South Caspian Basin and the Kura Basin of eastern Azerbaijan (Fig. 1). The Maikop Formation mudstones represent the geochemical record of the tectonic and chemical evolution of the basins from the time of their formation in the Eocene through to the mid-Miocene (Hudson et al., 2008; Popov et al., 2008; Van der Boon et al., 2015; Sachsenhofer et al., 2018). Events that may be geochemically identified include the uplift and unroofing of the Greater Caucasus Mountains, changes in sediment provenance and river volume inputs, and the restriction of basinal circulation patterns accompanied by development of bottom-water anoxia. Of particular interest to the development of petroleum reserves in the South Caspian Basin are factors controlling the development of anoxia and the subsequent preservation of organic material.

Maikop Formation deposition began around the time the Paratethys formed, which is generally thought to have been near the Eocene – Oligocene boundary (Popov et al., 1993; Rogl, 1999), though an earlier Paleocene – Eocene initiation has been proposed by some authors (Gaetani and Garzanti, 1991; Golonka, 2004; Kaz'min and Tikhonova, 2005). During initial formation of the Paratethys, open seaways existed to the west of the South Caspian Basin and possibly to the east which permitted marine circulation, thereby preventing water column stratification and the development of anoxia. Throughout the Oligocene and Miocene, these open seaways underwent periodic closure due either to a fall in eustatic sea-level or to regional tectonic activity, before becoming completely closed off during the Late Miocene (Popov et al., 2008; Hudson et al., 2008; Johnson et al., 2009).

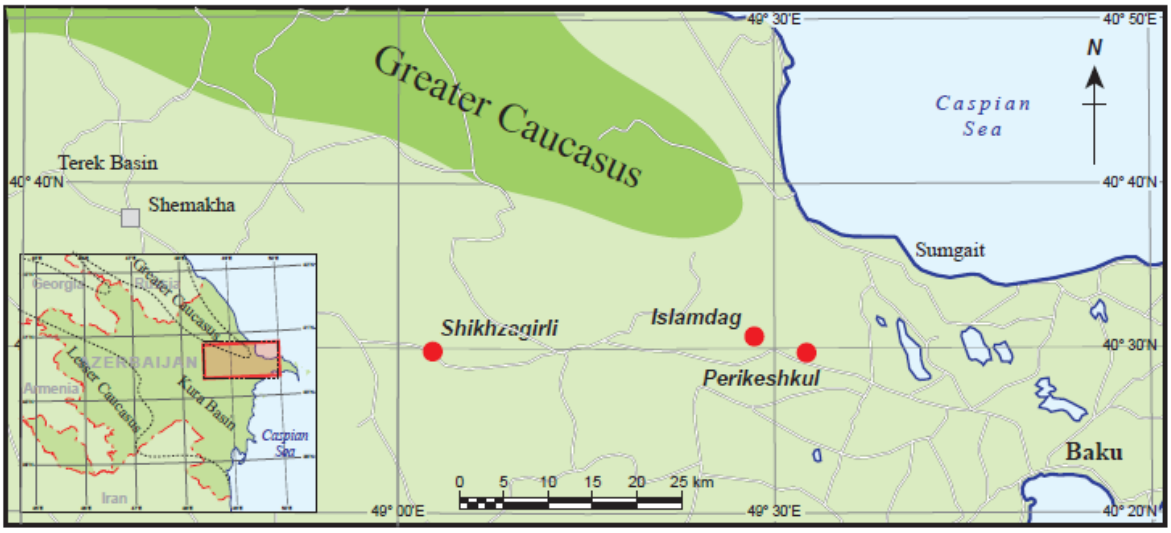

Fig. 2. Present-day geographical map showing the location of the study area in eastern Azerbaijan. The three sample sites are marked with red dots. Map modified from Hudson *et al.*, 2008.

Periods of isolation within the Paratethys are geochemically identifiable in the Maikop Formation mudstones via redox-sensitive trace metals including U, Th, Mo, V, Cr and Cu, and the abundance of organic carbon reported as Total Organic Carbon (TOC). Several studies seeking to identify anoxic events in the Maikop strata of eastern Azerbaijan have already been conducted (Hudson et al., 2008; Johnson et al., 2009; Bechtel et al., 2014); however, the results do not yield a consistent timing of deposition. The differences in timing may be due to major lateral variability in source rock parameters, or they may reflect problems with age dating (Sachsenhofer et al., 2018). The Maikop Formation is difficult to constrain using classical stratigraphic methods as it comprises a thick (up to 3km in the South Caspian Basin), homogenous package of mudstones which is nearly devoid of marker beds or diagnostic fossil assemblages.

Stratigraphy of the Maikop is further complicated by its deep burial in the South Caspian Basin. The age of initial Maikop deposition in the basin is debated, but the bulk of the sedimentary infill is attributed to deposits that are Oligocene and younger in age (Fig. 1, Brunet et al., 2003). Rapid sedimentation during the Pliocene to Quaternary deposited more than 10 km of sediment in less than 5 Ma on top of the Maikop Formation, thereby preventing the normal expulsion of fluids. As a result, the Maikop and much of the overlying Productive Series is overpressured and undercompacted (Narimanov, 1993; Brunet et al., 2003). Due to the depth of the basin and the overpressuring, no borehole penetrations to basement have been made, and continuous seismic correlation is lacking (Brunet et al., 2003). Therefore, previous stratigraphic studies of the Maikop have mostly been made by examining

outcrops at the margins of the Kura Basin, a sub-basin of the South Caspian Basin (e.g. Popov et al., 1998; Hudson et al., 2008; Johnson et al., 2010; Efendiyeva et al., 2012; Sachsenhofer et al., 2018) (Fig. 1).

Maikop strata in the Kura Basin are thought to be time-correlative with the Maikop strata in the deep South Caspian Basin (Johnson et al., 2009) although there are some differences. Maikop deposits in the much deeper South Caspian Basin are thought to consist of black shales in which there is a large amount of unoxidized carbon deposited under consistently anoxic conditions; whereas the Maikop in the Kura Basin was deposited in primarily oxic conditions with occasional suboxic-dysoxic episodes in discreet intervals (Johnson et al., 2009). Deposits in the Kura Basin are more proximal to the Greater Caucasus Mountains which may have been emergent during Maikop deposition, and are therefore closer to a sediment source.

The purpose of this study is to analyse samples of Maikop strata recovered from locations in the foothills of the Greater Caucasus Mountains in the Kura Basin, eastern Azerbaijan (Fig. 2), in order to build regional understanding of the Maikop as a petroleum source rock in comparison with nearby locations (see Pupp et al., 2018; Mirshahani et al., 2018). The geochemistry of the samples was studied to interpret their depositional setting and to identify potential anoxic episodes. Re-Os geochronology was used to obtain a numerical age date for the samples, and regional stratigraphic constraints were investigated using geochemical signatures and Re-Os isotope data. Some of this data has previously been presented in an extended Abstract (Washburn et al., 2018).

METHODS

Sample Collection

Samples were collected from three locations: Perikeshkul (40.497oN, 49.536oE), Mount Islamdag (40.514oN, 49.479oE), and Shikhzahirli (40.480oN, 49.076oE), as shown in Fig. 2. Selection of sample sites was based on previous work in which stratigraphic constraints drawn from microfaunal assemblages and chemostratigraphic data have been developed (e.g. Popov et al., 2008; Hudson et al., 2008; Johnson et al., 2009). At each sample site, dark intervals of mudstone potentially rich in organic matter were identified and sampled (Fig. 3).

Nine sample suites were recovered, each consisting of eight samples from a single lithostratigraphic horizon. Three sample suites were recovered from Perikeshkul, three from Mount Islamdag and three from Shikhzahirli. Two of the three sample suites at Perikeshkul were taken from pre-Maikopian strata (Fig. 3), in order to establish geochemical continuity throughout the stratigraphic section and to investigate a possible Os excursion during the Late Eocene (Dalai et al., 2006; Peuker-Ehrenbrink and Ravizza, 2012). All other samples are from Maikopian strata. From east to west, samples were taken from Perikeshkul (suites designated P-1 through P-3, stratigraphically oldest to youngest); Mount Islamdag (I-1 through I-3, oldest to youngest); and Shikhzahirli (S-1 through S-3, oldest to youngest), covering a lateral distance of about ~40 km, with the Perikeshkul and Islamdag sample sites only 10 km apart (Fig. 3).

Sampling was based primarily on meeting the needs of Re-Os geochronology. Rhenium and osmium are captured into organic-rich mudstones during deposition at the sediment-water interface under limited oxygen conditions (Cohen et al., 1999; Colodner et al., 1993; Crusius et al., 1996; Ravizza and Turekian, 1992; Ravizza et al., 1991). Incorporation of Re and Os into mudstones takes place by reductive capture into sediments and adsorption onto organic matter, with the majority of Re and Os becoming bound to organic matter (Cohen et al., 1999; Selby and Creaser, 2003; Yamashita et al., 2007; Georgiev et al., 2011; Rooney et al., 2012; Cumming et al., 2012). Some pre-existing Re and Os may be found in organic matter due to biogenic uptake during the lifespan of an organism (Rooney et al., 2016; Racionero-Gomez et al., 2017). Post-depositionally, the Re-Os system is robust and remains stable

through hydrocarbon maturation, and is even stable through contact metamorphism up to ~650 ˚C (Creaser et al., 2002; Rooney et al., 2010). However, Re and Os are both chalcophilic and siderophilic, and because they are bound to organic matter, they are susceptible to alteration through oxidative weathering and hydrothermal activity (Rooney et al., 2012; Kendall et al., 2009; Georgiev et al., 2012). Therefore, care was taken to avoid collecting samples showing any evidence of these processes.

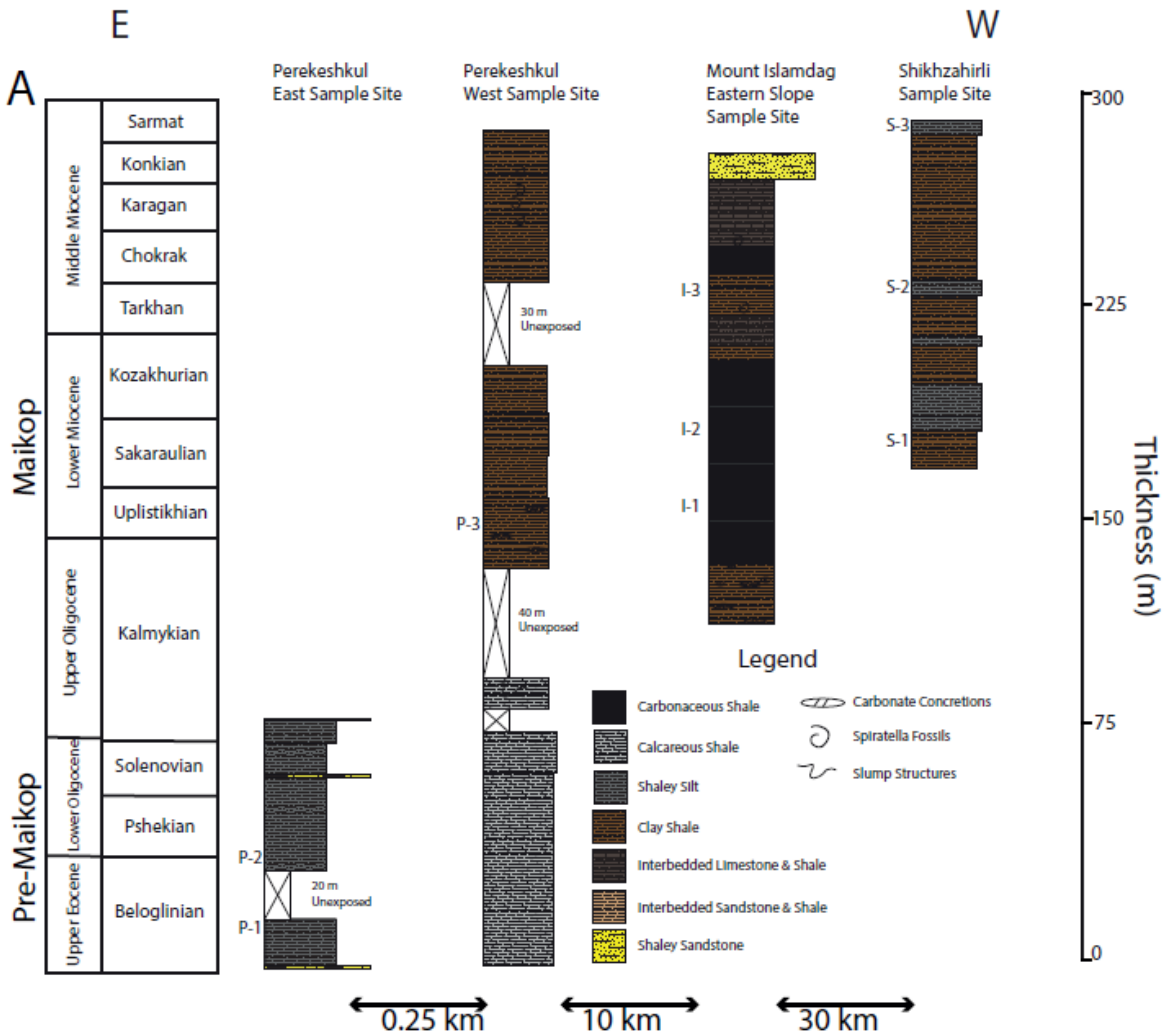

Fig. 3. Stratigraphic relationships shown between measured sections, spanning about 40 km laterally (see Fig. 1). Designated sample locations within the stratigraphy (P-1, I-1, S-1, etc.) represent intervals where at least eight samples were taken for Re-Os analysis. Perikeshkul and Mount Islamdag measured sections are from Popov *et al.* (2008). Figure modified from Popov *et al.* (2008).

After the identification of a potentially high TOC horizon (as identified by darker colour, high relative clay content, and knowledge gained through previous geochemical sampling at these localities as described in Hudson et al., 2008), a suite of samples was collected. At least six samples are required to produce enough isotopic heterogeneity between different samples to yield an isochron; but in order to account for the variable sedimentation rates in the Kura Basin, eight samples were recovered at each site to ensure sufficient heterogeneity to produce a statistically meaningful isochron. Due to the relatively short residence time of Re and Os, isotope heterogeneity was achieved by sampling along a single lamina set, limiting vertical variation between samples to 5 cm or less. Samples showing any sign of post-depositional alteration, such as fractures, rust stains, calcite veins and sulphur run- off, were not collected. The samples were dug out of the outcrops from a depth of 0.5 m in order to ensure that they

were not weathered. The samples typically weighed 50 to 100 g so that they could be ground and homogenized for analysis (Rooney et al., 2011).

Sample Preparation

All sample preparation for bulk elemental, trace element and pyrolysis analysis was conducted at Brigham Young University (BYU). Selected samples were crushed into small chips using a steel hammer, then powdered in a tungsten-ball mill. In order to ensure maximum surface area exposure for pyrolysis, samples were sieved through a US No. 40 Standard Test Sieve (425 µm).

Pyrolysis

Pyrolysis analysis was completed at BYU using a Wildcat Technologies Hydrocarbon Analyzer with Kinetics (HAWK) pyrolysis and TOC instrument. Samples were expected to have less than 10% TOC, so 50-70 mg of powdered sample was placed into a crucible for analysis as recommended by the manufacturer. In order to obtain total organic and carbonate carbon, as well as kerogen type and relative maturity, the samples were analyzed by whole-rock pyrolysis and total organic carbon/carbonate carbon (TOC+CC) techniques. A standard pyrolysis+TOC method was used where the sample was heated from 300oC to 850oC at a rate of 25o C/min. during the pyrolysis stage, and from 300oC to 850oC at a rate of 25 oC/min. during the oxidation stage (Espitalié et al., 1977; Peters and Cassa, 1994). Measurements included the amount of free hydrocarbons in the sample in mg HC/g rock (S1 peak); the kerogen yield, accomplished via the amount of hydrocarbons generated through thermal cracking of non-volatile organic matter (S2 peak); the organic carbon dioxide yield, i.e. the amount of CO2 in mg CO2/g rock produced during pyrolysis of kerogen (S3 peak); the mg carbon/g rock produced from the organic residue remaining after pyrolysis of kerogen is completed (S4 peak); the Tmax, the temperature at which the maximum generation of hydrocarbons from cracking of kerogen occurred during pyrolysis (measured at the S2 peak); the total organic carbon (TOC) in weight %; and the carbonate carbon (CC) in weight %. From these measurements, various parameters were calculated including the adsorption index, oil saturation index, hydrogen index, oxygen index, production index, generative organic carbon (weight %), and non-generative organic carbon (weight %). It is important to note that due to the mineral matrix effect, which refers to the interference of clay minerals with the release of hydrocarbons, pyrolysis results for samples with low TOC contents (<0.5 wt %) are qualitatively rather than quantitatively accurate (Peters, 1986).

X-Ray Fluorescence (XRF)

XRF analysis was performed using the Rigaku ZSX Primus II apparatus at BYU. For trace element analysis, samples were pressed into discs by combining 8.3 g of sample with 1.132 g of SpectroBlend 44 µm powder (composed of 81% C, 13.5% H, 2.9% O, and 2.6% N, with 0-10 ppm impurities of Ag, As, B, Cd, Hg, Pb and Sn). The sample mixtures were pressed to 50,000 lbs of pressure using tungsten pressing discs. For bulk element analysis, fused disc samples were prepared by combining 1.23 g of sample with 8.61 g of lithium borate flux, then fused using a platinum crucible in a Katanax K1 fused disc preparation machine. In order to ensure proper machine operation, samples were analyzed along with standards JA-1 (andesite from Japan), JA-2 (andesite from Japan), SGR-1 (mudstone from the Green River Formation), JB-1A (basalt from Japan), JR-1 (rhyolite from Japan), and RGM-1 (rhyolite from Glass Mountain). Major and minor elements analyzed via XRF include Si, Ti, Al, Fe, Mn, Mg, Ca, Na, K, P, Ba, Ce, Cr, Cu, Ga, La, Nb, Nd, Ni, Pb, Rb, Sc, Sm, Sr, Th, U, V, Y, Zn and Zr.

Leco Sulphur Analysis

Sulphur analysis was conducted using a Leco Furnace Sulfur Analyzer at the ALS Canada geochemistry laboratory, British Columbia. Some 0.01 to 0.1 g of each sample was heated in the Leco

furnace to approximately 1350˚ C while passing a stream of oxygen through the sample. Sulphur dioxide released was measured by an infra-red (IR) detection system to measure the total sulphur released from the sample.

Inductively Coupled Plasma Optical Emission Spectrometry (ICP-OES)

In order for samples to be accurately analyzed in the ICP-OES, they were first homogeneously dissolved into solution. Samples were prepared for acid digestion by powdering the fused discs used in XRF analysis (see Ingamells, 1970). As aluminum had been analyzed in the XRF, the discs were powdered in an alumina- ceramic shatterbox in order to avoid contamination with elements not yet analyzed (specifically Co, with which tungsten shatterboxes are contaminated). Powdered discs were dissolved in an acid solution containing 0.7 g of sample, 20 g of 10% HCl solution, 10 drops of 10M HNO3, and approximately 30 g of milli-Q water to a total volume of 50 mL (~50g).

Samples were then analyzed using a ThermoScientific iCAP 7400 ICP-OES in the laboratory of BYU. Standards run along with samples were JA-2 and SGR- 1, which were prepared for ICP-OES using the same process. Crossover data between the XRF and ICP- OES was compared and determined to be within a few percent error. Elements analyzed via ICP-OES include Mo, Co and As. Other elements resulting from ICP- OES analysis were used to verify the measurements performed via XRF, including for Ba, Cr, Cu, Ni, Sr, V and Zn.

Re-Os Analysis

As Re and Os are associated with the deposition of organic matter and a relationship between Re and Mo contents can often be shown, samples to be analyzed for Re-Os geochronology were selected based on TOC values, the abundance of molybdenum, and current stratigraphic constraints. In order to minimize sample contamination, selected samples were polished using silica carbide grit pads to remove surfaces potentially exposed to surface weathering and that may have been contaminated by metal tools. Samples were then broken into pieces in a ceramic mortar and pestle, and powdered in an alumina-ceramic shatterbox to yield 30-80 g of powdered sample.

The detrital component of Os in organic-rich mudstones causes an increase in scatter around the isochron. In order to minimize this scatter and increase the accuracy of the Re- Os geochronometer, a digestion method that limits the removal of any detrital Re and Os component was employed. The digestion method used was detailed in Selby and Creaser (2003). In this method, whole-rock powders are reacted with a Re-Os purified digestion medium of CrO_3 in 4 N H_2SO_4 (0.2 g CrO_3 per ml of 4 N H_2SO_4). Approximately 1 g of each sample with less than or greater than 5% TOC was digested in 8 mL or 16 mL of CrO_3- H_2SO_4 solution, respectively, together with a mixed tracer solution of ^{185}Re and ^{190}Os in a sealed Carius tube at 240˚ C for 48 hours. Following acid digestion, Os was isolated from the solution using $CHCl_3$ solvent extraction and micro-distillation. Following the Os extraction, Re was isolated and purified using NaOH-Acetone solution extraction and anion chromatography.

Due to the high ionization potential of Re and Os (~9eV, Dickin, 2008), samples were analyzed using negative thermal ionization mass spectrometry (NTIMS) in a Thermo Scientific Triton TIMS instrument. Analysis via N-TIMS allows measurement of Re and Os at the nanogram to sub-nanogram concentration, respectively, with accuracy up to ±0.5% 2σ (Völkening et al., 1991; Creaser et al., 1991). The purified fractions of Re and Os were loaded onto Ni and Pt wire filaments, with the Re isotope compositions determined via static Faraday collection, and the Os isotope compositions obtained via peak hopping using a secondary electron multiplier. For the $CrVIO_3$–H_2SO_4 solution, total procedural blanks during this study were 18.0 ±3.0 pg and 0.20 ± 0.05 pg (1 S.D., n = 4) for Re and Os, respectively, with an average $^{187}Os/^{188}Os$ value of 0.17 ± 0.05 (n = 4).

Statistical Analysis

Bulk geochemical data were analyzed statistically to produce a clustering of samples and geochemical element abundances using JMP Pro 13 software. In JMP, statistical hierarchal clustering was achieved through the calculation of a Cubic Clustering Criterion (CCC). Calculating the CCC involves plotting sample results on a hypercube containing a uniform distribution of reference points, then using a heuristic formula to estimate the error of a distance (between reference points and actual points) based clustering algorithm in the reference distribution. For this study, Ward's method (see Wilks, 2011) was used, where the distance is calculated as:

$$D_{KL} = \frac{\| \bar{x}_K - \bar{x}_L \|^2}{\frac{1}{N_K} - \frac{1}{N_L}}$$

where D_{KL} is the distance from cluster C_K to C_L; C_K is the Kth cluster; x_K is the mean vector for cluster C_K; and N_K is the number of observations in C_K. A high value of the CCC corresponds to a smaller error (as calculated by R2); therefore, the higher the CCC, the more reliable the clusters. Using the CCC, a number of clusters were chosen which are statistically and geologically reasonable. Samples were divided into seven clusters with a CCC of 18.47, which was the highest value of CCC calculated between varying numbers of clusters.

Clusters were then plotted on a dendrogram to display their relative relationships to each other. Line distances in the dendrogram correspond to distances between clusters, and therefore display the mathematical similarity between geochemical signatures. The dendrogram was also plotted with two-way clustering in order to show element relationships, and a heat map was plotted to visually represent the element clustering between samples. Using the dendrogram, improved correlations between geologic units in the measured sections of the Maikop Formation in Eastern Azerbaijan were drawn.

RESULTS

The purpose of the geochemical analyses was to provide geochemical constraints on intervals of Maikop strata that could be used for regional correlation together with a numerical age datum from Re-Os geochronology. Results for organic matter content, detrital input, anoxic indicators and Re-Os geochronology will be discussed separately in the following section, along with a description of the statistical relationships between geochemical indicators.

Organic matter preservation and type

The TOC content in samples from the seven Maikopian- aged sample suites within the Kura Basin is generally low (~1% average), with the exception of samples taken from Islamdag (~3% average, Fig. 4a; Table 1). A cross-plot of Tmax versus HI (Fig. 4b) shows that much of the preserved kerogen is terrigenous Types III and IV material. However the lower two sample suites from Islamdag (I-1 and I-2) and the P-3 sample suite from the western Perikeshkul site contain mixed Type II/III kerogen and, in the case of the middle Islamdag sample suite, predominantly marine (Type II) kerogen (Fig. 4b).

The palaeo-proxy elements Cu and Ni showed a good correlation with TOC, indicating that significant post-depositional organic matter degradation has not taken place (Fig. 5a, b) (c.f. Huerta-Diaz and Morse, 1992; Fernex et al., 1992; Nameroff et al., 2002, 2004; Piper and Perkins, 2004; Algeo and Maynard, 2004; Tribovillard et al., 2006). Thus measured TOC probably closely represents the original depositional organic matter content of the samples; this is further supported by low Tmax and Production Index (PI) values for the sample suites (Table1).

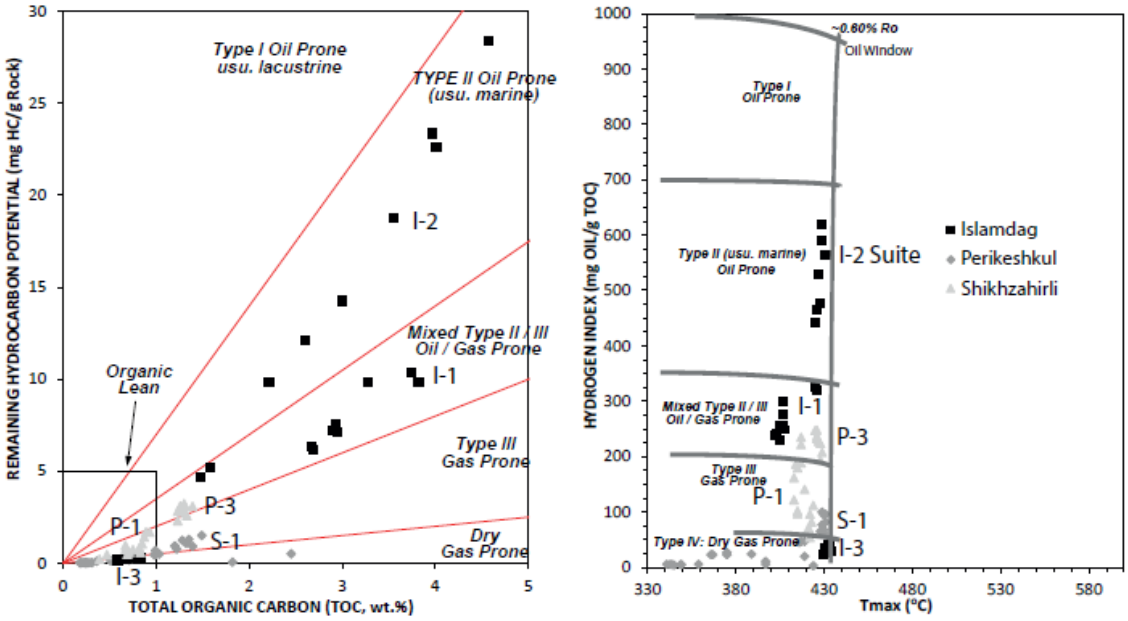

Fig. 4. (Left) Total organic carbon (TOC) and remaining hydrocarbon potential based on the results of HAWK pyrolysis. Sample suites (8 samples each) are marked near their clusters (see Fig. 3). (Right) Maturity of hydrocarbons in samples based on Hydrogen Index versus T_{max} from HAWK pyrolysis.

Detrital Input

Primary detrital indicators in the samples include Ti, Al, Ga, La and Sc as these elements are typically bound in minerals which are resistant to degradation (Table 2; Kryc et al., 2003; Tribovillard et al., 2006; Wood and Samson, 2006). Good correlations are observed on cross-plots between each of these elements (Fig. 6a-d) thereby confirming their detrital nature and indicating minimal authigenic enrichment of these elements. The detrital elements are reported in Fig. 6 as enrichment factors, which involves presenting elemental concentrations relative to the concentrations in a reference material composed of average shale (Wedepohl, 1971).

Overall and with a few exceptions, the samples are depleted in detrital elements. Enrichment factors calculated from average black shale compositions (Wedepohl, 1971, 1991) show that the P-1, P-2, I-2, S-1, S-2 and S-3 sample suites are depleted (or near- depleted) in Ti, with Al enrichment ranging from 0.60 to 1.20 for these samples. Enrichment of both Ti and Al appears to be most significant in the P-3, I-1 and I-3 sample suites, which showed average enrichment factors of Ti and Al of 1.00-1.20 and 1.20-1.60, respectively (Fig. 6a).

Ga, La and Sc are typically bound in minerals with low solubility (e.g. bauxite) and correlate well with Ti and Al in the samples analysed (Figs 6b-d). They were therefore used to support the abundance of detrital influx (Wood and Samson, 2006). Similar values of enrichment are observed in the sample suites, with the greatest enrichment of La, Ga and Sc in the I-3 and P-3 sample suites (1.0, 1.40 and 1.60, respectively; Figs 6b-d).

Anoxic Indicators

Elemental indicators for anoxia include U, Th, Mo, V, Cr, Ni, and Cu. Abundances of these elements were plotted on bivariate diagrams using elements and element ratios (Fig. 7a-e).

The sample suites from Perikeshkul and Shikhzahirli showed enrichment factors of Mo <20 (Fig. 7e), U/Th ratios <0.75 (Fig. 7a, b), V/Cr ratios <2.00 (Fig. 7b), and had generally low values of TOC (~1 wt % average TOC) (Fig. 7c, d, e; Table 1). The values of these ratios and the enrichment factor of Mo

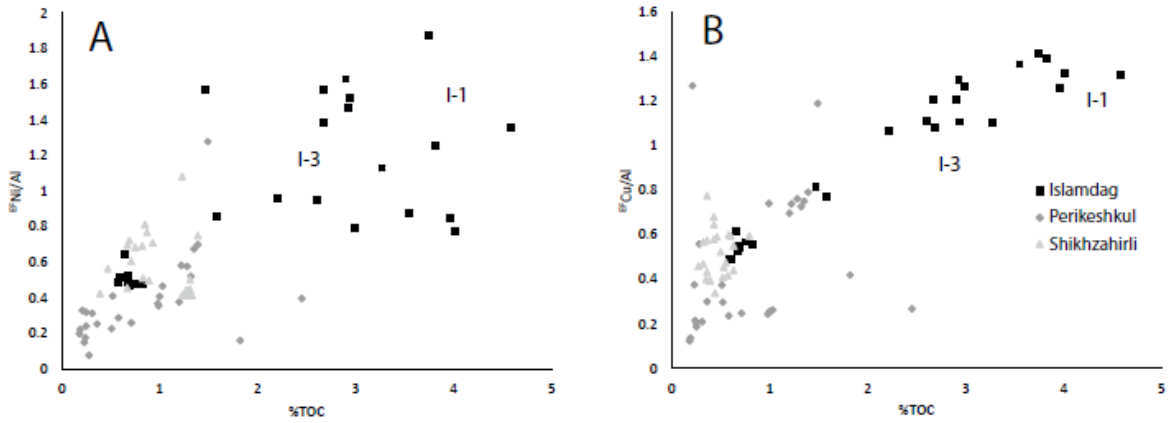

Fig. 5. Plots showing enrichment factors for Ni and Cu in comparison to TOC. Cu and Ni are bound in organic matter either while the organism is alive or after death at the sediment-water interface. Significant degradation of organic matter below the sediment-water interface results in authigenic mineral formation, leading to enrichment of Cu and Ni relative to TOC. A strong linear trend between Cu, Ni and TOC likely indicates that limited organic matter degradation has taken place below the sediment-water interface.

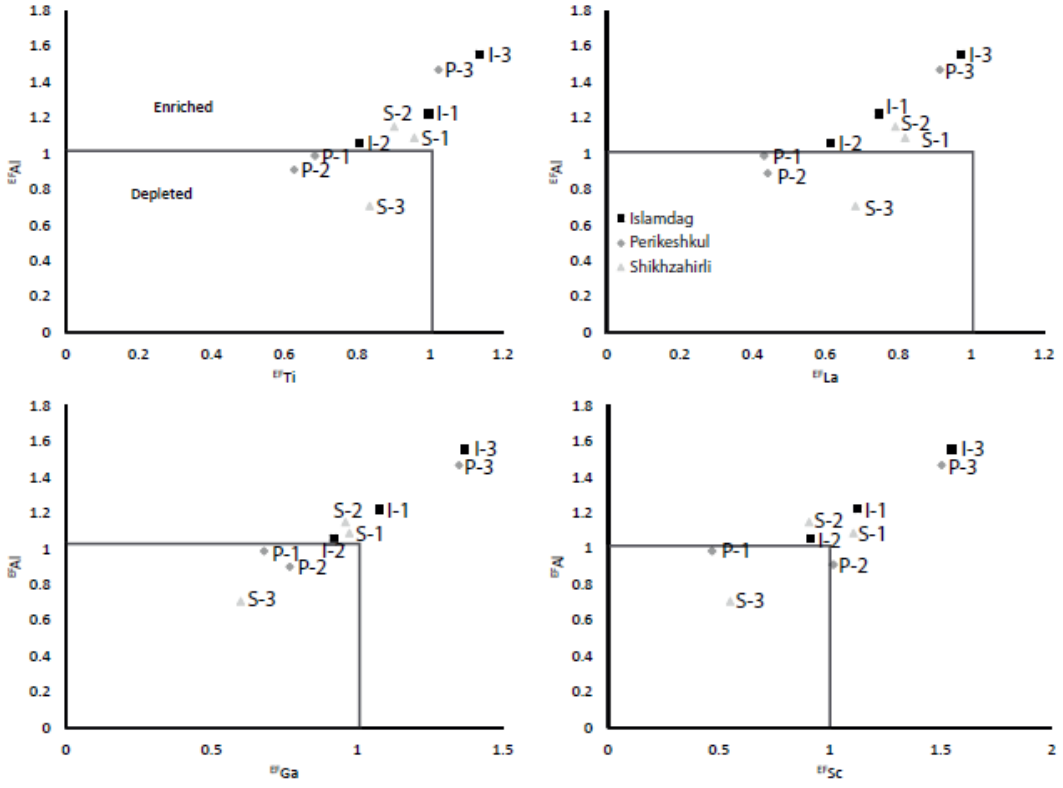

Fig. 6. Enrichment factors of elements (Ti, La, Ga and Sc) typically bound in insoluble, weathering-resistant detrital minerals that may be used as proxies for relative detrital input. Absolute values shown in Table 2 have been converted to enrichment factors relative to reference shale values (Wedepohl, 1971; 1991). Values above 1 (outside of black box) are considered to indicate enrichment in detrital elements, while those below 1 are considered to indicate depletion. The values therefore indicate the relative amount of detrital input into the system for each sample suite.

suggest that the samples were deposited in oxic conditions (c.f. Jones and Manning, 1994) (Fig. 7a, b). When comparing values of TOC with Al- normalized enrichment factors of Cu, Ni, U, Va and Mo, no

correlation was observed, also indicating deposition in oxic conditions (c.f. Tribovillard et al., 2006).

Two of the sample suites from Islamdag follow these trends; however, one sample suite from Islamdag (sample Suite I-1) has average EFMo >50, U/Th values >1.25, V/Cr values between 2.00 and 4.25, and average TOC of 4 wt % (Fig. 7). These values indicate that this sample suite was deposited in suboxic to anoxic conditions (c.f. Jones and Manning, 1994). Comparisons of TOC with enrichment factors of Al-normalized Cu, U and Mo show a weak overall correlation, but a significantly higher relative enrichment, likewise indicating that the sample suite was deposited in suboxic to anoxic conditions. The results of organic preservation throughout the sample suites presented here are similar to those in previous studies (Hudson et al., 2008; Johnson et al., 2009).

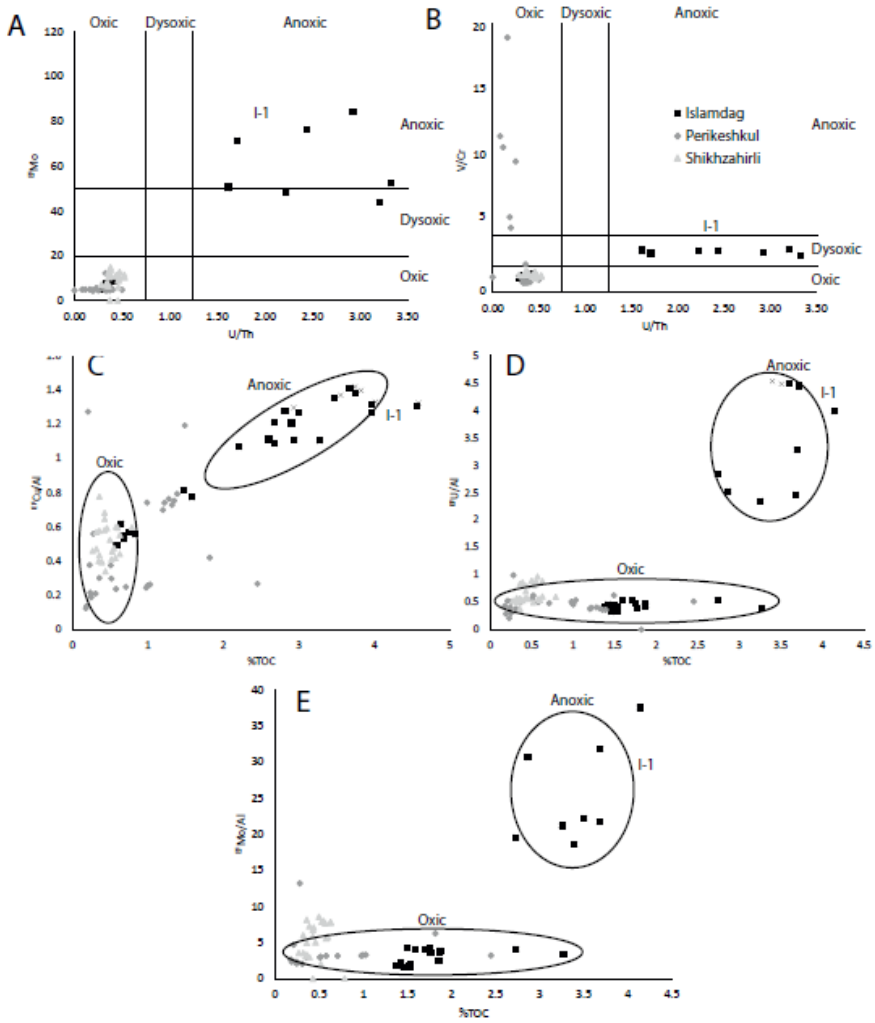

Fig. 7. Oxic and anoxic geochemical indicators. (A) and (B) are quantitative anoxia indicators from Jones and Manning (1994). (C), (D) and (E) are qualititative geochemical indicators of anoxia from Tribovillard *et al.* (2006). With small variations, most geochemical indicators agree that all of the Maikop samples collected from the Kura Basin were deposited in oxic bottom-water conditions, save for the I-1 sample suite from Islamdag, which consistently plots in anoxic to dysoxic bottom-water conditions.

Re-Os Geochronology

Of the five sample suites analyzed for Re-Os geochronology (P-1, P-3, I-1, I-3, and S-1), only one Re-Os data-set successfully produced a meaningful age and uncertainty: the Islamdag I-1 sample suite (Fig. 8A, B, C). The Islamdag I-1 samples possess 187Re/188Os and 187Os/188Os values of between

~2000 and 6000, and ~1.0-2.3, respectively (Fig. 8a, b, c) which are positively correlated. The sample set yielded an Re- Os date of 17.2 ± 3.2 Ma, with an initial 187Os/188Os of 0.71 ± 0.23 (Fig. 8a). However, significant scatter is exhibited by the data-set about the best-fit line, as described by the high mean square of weighted deviates (MSWD) value of 660. The scatter could be the result of post-depositional disturbance to the Re-Os system, and/or variability in the initial 187Os/188Os composition of the sample set.

With initial 187Os/188Os values calculated at 17.2 Ma, the sample set describes two subsets which plot above and below the best-fit line and which yield initial 187Os/188Os values of ~0.80 and ~0.56, respectively (Fig 8b-c; Table 3). The two subsets yield Re-Os dates of 16.9 ± 2.2 Ma (initial 187Os/188Os = 0.80 ± 0.14, MSWD = 33) and 18.3 ± 1.7 Ma (initial 187Os/188Os = 0.56 ± 0.13, MSWD = 21) (Fig. 8b, c). These age-date determinations are identical within the limits of uncertainty. Samples that fall above and below the best-fit line of the complete data-set do not appear to be related to any stratigraphic cyclicity, and other geochemical data does not mirror the same pattern. The lack of stratigraphic grouping of samples with variable initial Os indicates that the variation in initial Os cannot be due to a single change in depositional conditions.

The sample suites at S-1, P-1, I-3, and P-3 all failed to produce statistically meaningful Re-Os geochron ages. Possible causes for isochron failure include the low concentration of radiogenic Re and the relatively young geologic age of the samples.

Stratigraphic Correlations

Hierarchal clustering statistics confirmed that samples within any one suite represented a single lithologic unit, as the samples in each suite were found to be nearly geochemically identical. Relationships between the geochemistry of sample suites were quantified by hierarchal clustering analysis and were represented on a hierarchal diagram on which the geometric appearance of the diagram is mathematically determined (Fig. 9). Previous studies (Hudson et al., 2008; Johnson et al., 2009) suggested that the three sample localities expose much of the same stratigraphy and this is consistent with the geochemical comparison of the samples in this study.

Bulk geochemical analyses indicate a moderately strong relationship between the lower Islamdag (I-1) and upper Perikeshkul (P-3) sample suites (Fig. 9). A similarly strong relationship exists between the S-1 and S-2 sample suites from Shikhzahirli, which in turn are shown to have a moderately strong relationship to the I-3 sample suite.

The P-2 and S-3 sample suites show a moderate relationship that is likely related to similarities in mineralogy and depositional conditions, as they are not likely to be related stratigraphically (Fig. 9). The other sample suites, including the P-1 and I-2 suites, are only weakly related to the other sample suites, indicating different depositional conditions and / or sediment supply.

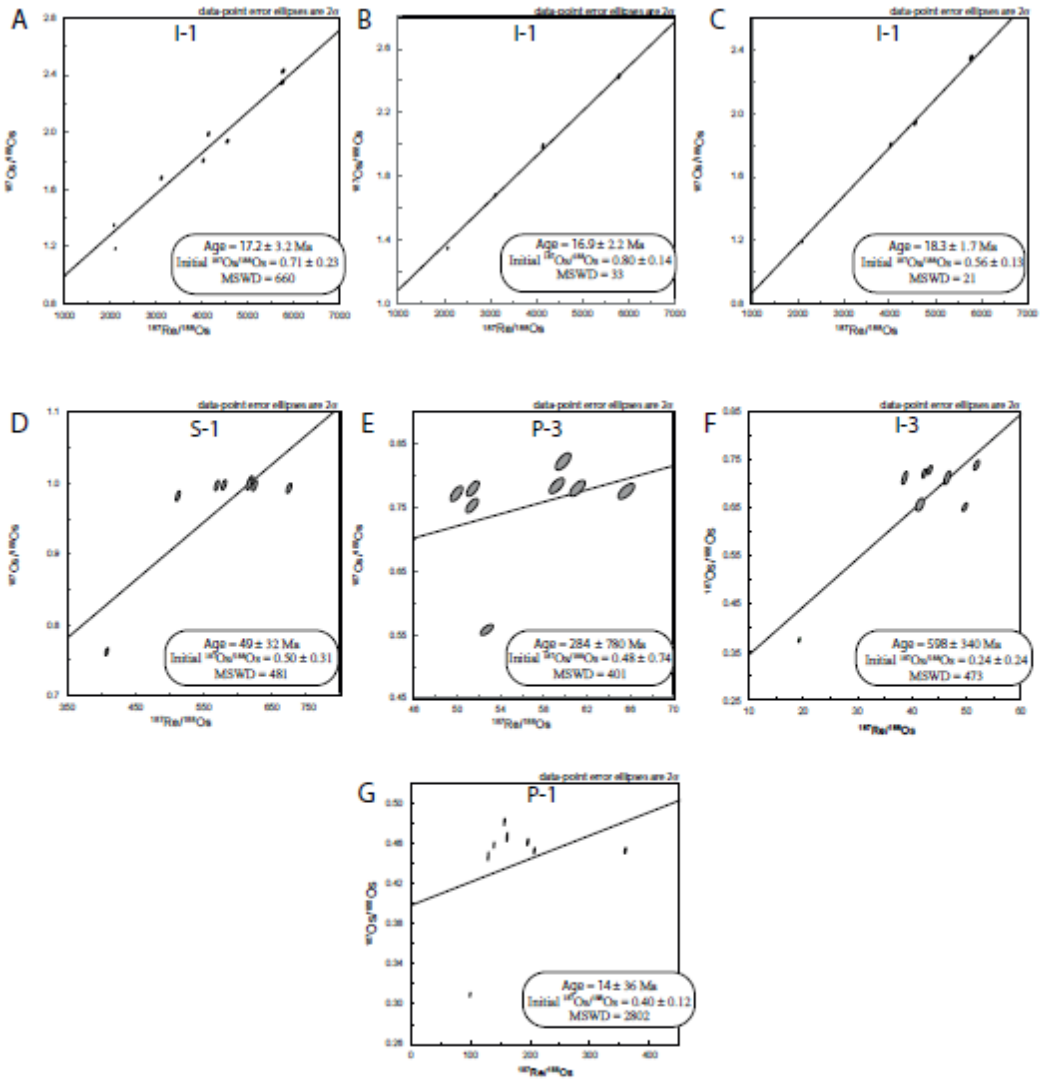

Fig. 8. $^{187}Re/^{188}Os$ versus $^{187}Os/^{188}Os$ plots. The Re-Os data from the I-1 sample suite yielded the only meaningful age determinations (A, B, C). (A) displays the solution using the full sample suite from I-1. Using the full suite, the best-fit of the data shows considerable scatter (see text for discussion). However, the distribution above and below the isochron led to the division of the I-1 sample suite in to two sub groups (B, C). The two sub-groups yielded a Re-Os date within uncertainty. D, E, F, G: $^{187}Re/^{188}Os$ versus $^{187}Os/^{188}Os$ plots for the sample suites studied for Re-Os geochronology. These four sample suites failed to produce statistically meaningful Re-Os isochrons, and the subsequent initial $^{187}Os/^{188}Os$ calculated from the failed isochron is erroneous.

DISCUSSION

The results of this study indicate that, despite its ability to generate large volumes of oil and gas, the majority of the analyzed Maikop samples from the Kura Basin may not have been deposited in anoxic settings, in agreement with the conclusions of Hudson et al. (2008) and Johnson et al. (2009). The majority of the analyzed samples are low in TOC (<1%), and organic matter is mainly terrigenous. Only the Islamdag lower and middle sample suites (suites I-1 and I-2: Fig. 3) had significant TOC contents (up to 5%).

Geochemical analyses indicate that the lower Islamdag sample suite contains mixed terrigenous and marine organic matter (Fig. 4), the preservation of which was likely due to suboxic to anoxic depositional conditions. Although the middle Islamdag suite had similar TOC values, geochemical

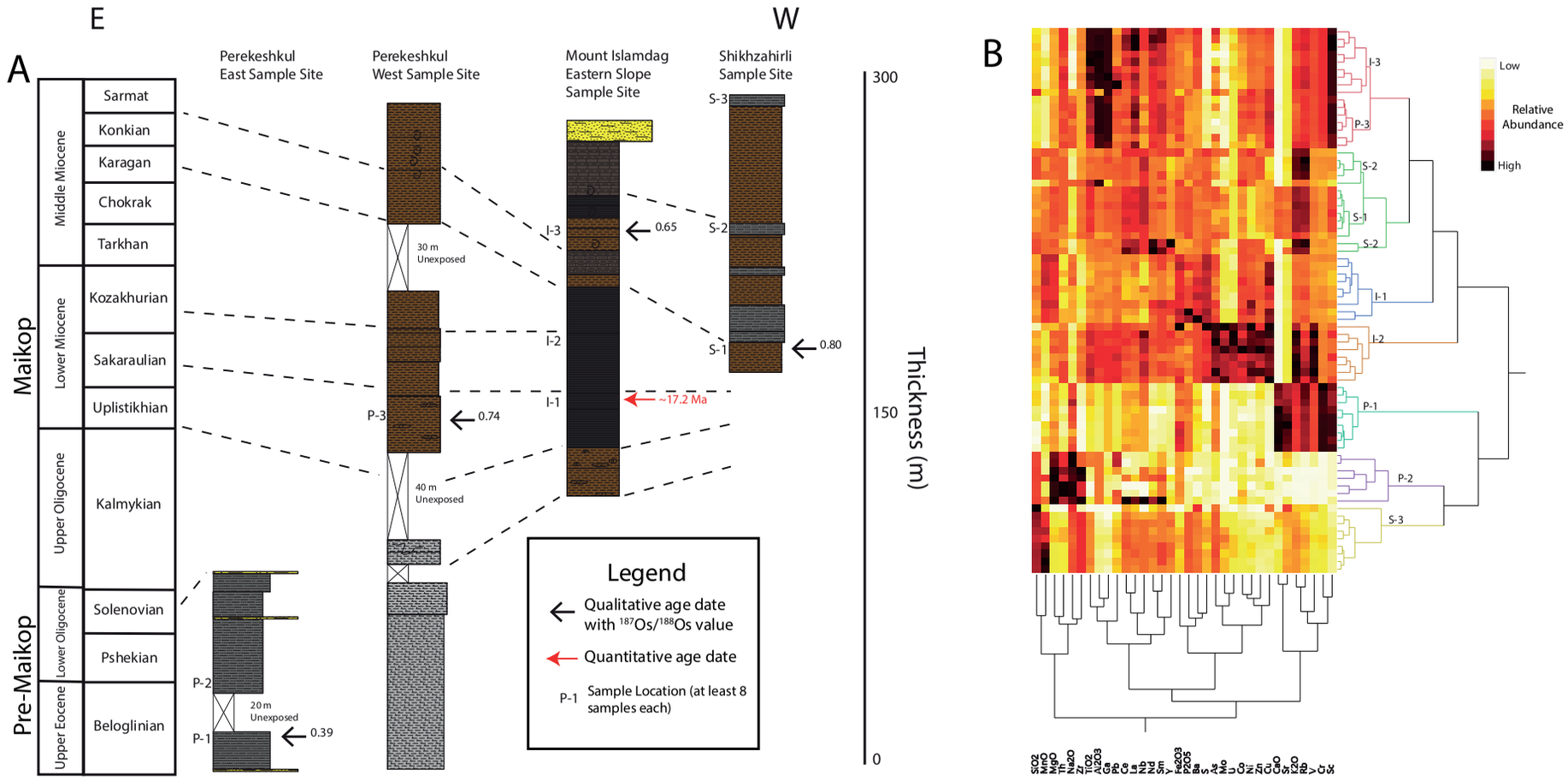

Fig. 9. (A) Stratigraphic correlations of sample site measured sections, modified from Popov *et al.* (2008). Five sample suites were measured for Re-Os geochronology. Of the five, one (I-1) produced an isochron date of ~17.2 Ma. The other four are dated qualitatively using the global seawater curve for $^{187}Os/^{188}Os$ compiled by Peuker-Ehrenbrink and Ravizza (2012; see Fig. 10). Each sample suite location refers to eight samples taken from a single lithologic unit. Stratigraphic correlations are based on microfaunal assemblages (Popov *et al.*, 2008), geochemical statistical clustering analysis, and Re-Os geochronology. (B) Geochemical two-way cluster analysis displaying statistically determined relationships between sample suites and the elements analysed for each sample. Clustering was determined using cubic clustering criterion (see Equation 1).

analysis indicated the presence of dominant marine organic matter deposited in oxic conditions. The preservation of organic matter was likely due either to high productivity rates which outpaced organic matter degradation at the sediment- water interface, to high sedimentation rates, or to a combination of both factors.

Re-Os geochronology, though only successful for the I-1 sample suite, provides important new age-data which is relevant for both the South Caspian and Kura Basins. An age date of ~17.2 Ma for the lower Islamdag sample suite (Fig. 8a) provides a reference datum for the bio-, chemo-, chrono- and lithostratigraphic data which has previously been collected throughout the basins (Washburn et al., 2018). This age date is in contrast to earlier estimations by Hudson et al. (2008), Johnson et al. (2009) and others, which were based upon sparse biostratigraphic control and chemostratigraphic correlation, which suggested the lower portion of the Islamdag outcrop was Oligocene in age. This is an important finding – the Islamdag outcrops are often used for both academic research and as a teaching outcrop for those working the Maikop Formation, and some previous interpretations as to the age of these strata have been shown to be incorrect through this work.

Though the age data obtained from the I-1 sample suite carries a high degree of confidence, there are two puzzling aspects of the isochron produced for this lowermost Islamdag sample suite. The first is the production of two isochrons of identical date (within error) but differing initial $^{187}Os/^{188}Os$ composition. The reason for the split is unknown, as other elements analyzed in this study do not show the same separation pattern between samples. It may be possible that the differences are the result of rapid changes within the hydrodynamic system in the basin at the time of deposition. These changes may be the result of increased and decreased restriction of the greater South Caspian Basin caused by regional tectonics and/ or relative sea level changes. Additionally, the lower value for initial $^{187}Os/^{188}Os$ of 0.56 suggests that sediment being supplied to the basin contained a lower fraction of radiogenic isotopes, indicating a mainly volcanic provenance area such as the volcanic Talysh Mountains to the south of the Kura Basin (Fig. 1). The volcanic rocks and volcanogenic sediments in the Talysh are mainly high-K alkali basalts that were emplaced throughout the Paleocene to the Eocene.

The second puzzling feature of the Re-Os data from the lower Islamdag suite is the anomalously high enrichment in Os and Re, with higher values than any previously published. Thus values for this sample suite are ~600 ppt, whereas the highest values published from any other sample are only about one-half of that, or ~300 ppt, as represented by ^{192}Os (sample suite I-1; Table 3: page 299). This could be due to the more efficient uptake of Os into organic matter; the higher preservation of organic matter past the sediment-water interface which allowed for more authigenic enrichment of Os; an increased supply in Os due to oxidative weathering of Os-rich minerals; or a combination of these factors (Ravizza and Esser, 1993; Selby and Creaser, 2003; Baioumy et al., 2011; Cumming et al., 2012).

The failure of the other sample suites to produce an isochron was due to the lack of heterogeneity in the $^{187}Os/^{188}Os$ versus $^{187}Os/^{188}Os$ compositions between collected samples. The mechanisms producing heterogeneity of Re and Os between samples are not fully understood (Ravizza and Turekian, 1989; Creaser et al., 2002; Georgiev et al., 2012; Cumming et al., 2012; Harris et al., 2013). Lack of heterogeneity may have come about through disturbance of the Re-Os system through oxidative weathering; through differences in Re and Os uptake between sample sites due to variations in water-column chemistry or organic matter type; as a result of differences in sedimentation dynamics; or due to insufficient spacing of sampling, vertically or horizontally. As the potential for oxidative weathering in outcrop samples cannot completely be ruled out, future studies should seek to obtain Re-Os isochrons from core samples.

Despite the lack of isochrons, it is still possible to derive some depositional control from the initial $^{187}Os/^{188}Os$ ratios. Osmium isotope ratios for sample suites provide qualitative control on either basin dynamics (at times the basin was restricted) or depositional age (at times the basin was in open communication with the open ocean), based on correlation, or lack thereof with the global seawater

187Os/188Os curve (Peuker-Ehrenbrink and Ravizza, 2012). For example, the I-1 suite (dated at ~17.2 Ma) has an average initial 187Os/188Os ratio of 0.71 (Osi @ XX myr, Table 3). This calculated initial 187Os/188Os value falls below the global sea level curve (Fig. 10), indicating that the basin was not in perfect communication with the open ocean. This is consistent with indications of bottom water suboxia/anoxia (Figs 5, 7), and in agreement with geochemical data from this study and others that suggest periodic, limited basin isolation during the Oligocene-Miocene (Hudson et al., 2008). Sample suite I-3, stratigraphically above suite I-1, also plots below global values (Fig. 10), also suggesting basin restriction. While not all anoxic indicators suggest basin restriction for this sample suite, elevated TOC, EFCu/Al and EFNi/Al (Figs 5, 7) are consistent with decreased oxygen availability at this time.

In contrast to the sample suites analysed at the Islamdag locality, the initial 187Os/188Os values for the P-3 and S-1 sample suites appear to correspond to global oceanic values very well. Average values for the two sample suites are 0.74 ± 0.004 and 0.80 ± 0.05, respectively, with initial values calculated between 12 and 22 Ma. These higher average values correspond with the global 187Os/188Os curve from the late Middle Oligocene through the late Middle Miocene (Fig. 10). We interpret these sample suites to indicate good connectivity between the Kura Basin and the open ocean.

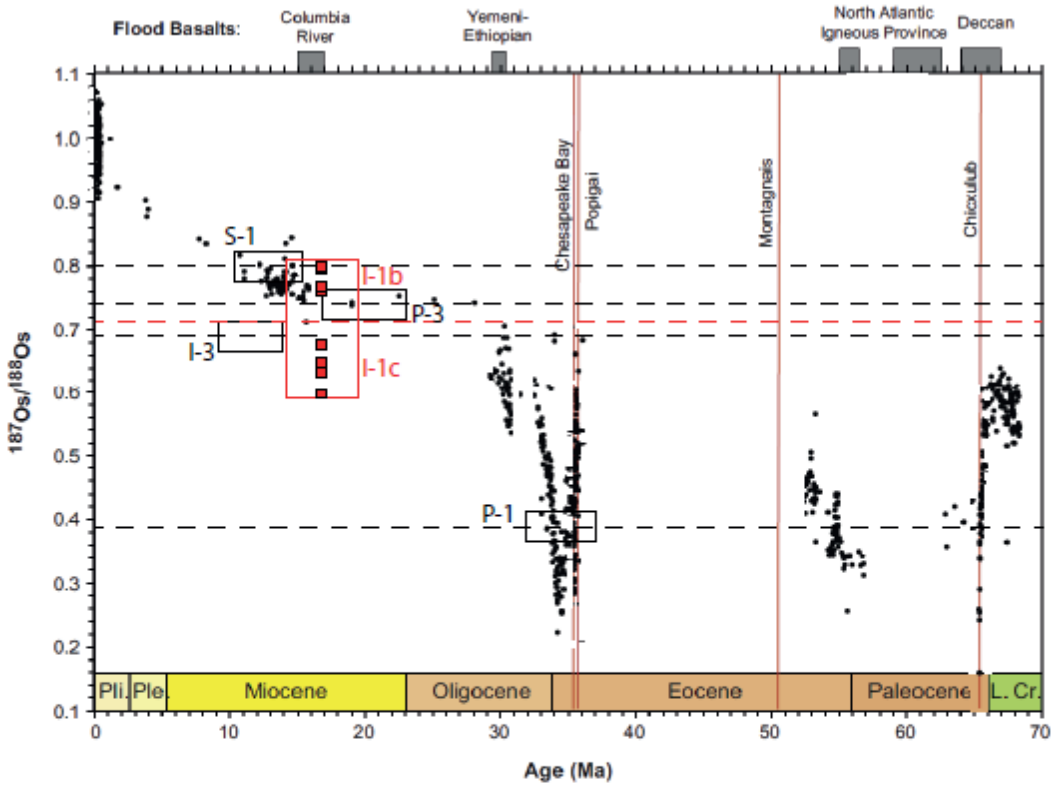

Fig. 10. Marine $^{187}Os/^{188}Os$ record of the past 70 million years, compiled by Peuker-Ehrenbrink and Ravizza (2012). Initial $^{187}Os/^{188}Os$ values of sample suites are compared to the record to estimate qualitative age dates. Good correlation of sample values to the global oceanic curve suggests connectivity between the Kura Basin and the open ocean, while significant divergence from the global curve suggests basin restriction. Dashed lines represent average initial $^{187}Os/^{188}Os$ values for the sample suites analysed (Fig. 2). Boxes represent interpreted qualitative ages of deposition based on stratigraphic relationships to the successfully produced isochron and the matching of the initial $^{187}Os/^{188}Os$ to the global seawater curve. Within the red box representing sample suite I-1, the red squares represent individual values for each of the eight samples from the I-1 sample suite, with the I-1b and I-1c sub-suites plotting in discrete groups. The I-1b values plot within the range of global oceanic averages, but the overall average of 0.71 for suite I-1 (red dashed line) is below the global average, as are the I-1c values, suggesting restriction of the Kura Basin during deposition at the Islamdag locality.

When comparing the four sample suites discussed above, each of which indicates a Miocene age, some of the suites suggest a connection to the open ocean (those from Perikeshkul and Shikzagirli) while others suggest restriction (Islamdag). This is not a new observation – geochemical spatial trends have been reported in the Kura Basin in previous studies, with enrichment in anoxic trace metals and organic matter preservation (TOC) increasing generally to the NW and showing elevated values at Islamdag (Hudson et al., 2016). This further reinforces the idea that spatial variability may play a much larger role in the shallower, more spatially constrained Kura Basin in contrast to the much deeper, less restricted South Caspian Basin to the east.

The fifth sample suite, P-1, is considered to be the oldest, and is interpreted to consist of pre-Maikopian rocks that were deposited near to the Eocene – Oligocene transition (Hudson et al., 2008). The P-1 sample suite has an average initial $^{187}Os/^{188}Os$ ratio of 0.39 ± 0.15, which was calculated assuming an age of 39 to 29 Ma. This low $^{187}Os/^{188}Os$ value correlates well with the osmium isotope excursion at the Eocene- Oligocene Transition (EOT), as discussed by Dalai et al (2006) and reflected in the global $^{187}Os/^{188}Os$ sea level curve (Fig. 10). The agreement between this sample suite and values reported for the EOT elsewhere indicates that the basin was connected to open-ocean waters during deposition of this pre-Maikopian interval, consistent with a general understanding of the evolution of the South Caspian Basin.

The majority of sample suites from this study exhibit low enrichment factors for detrital indicators, suggesting that sedimentation rates were relatively low in the Kura Basin in comparison to the South Caspian Basin to the east. This is reinforced by Re-Os geochronology – interpreted ages of the I-1 and I-3 sample suites suggest a sedimentation rate of 2-4 cm/ ka based on the ~100 m of strata between the two at this locality. However, two sample suites showed more significant enrichment in detrital indicators – Islamdag I-3 and Perikeshkul P-3, with enrichment averages of 1.0-1.20 and 1.20-1.60 for Ti and Al, respectively (Fig. 6). These samples show the increasing influence of the nearby Greater Caucasus during the Miocene (Ershov et al., 2003; Saintot et al., 2006; Vincent et al., 2007), an event that we propose is responsible for the spatial and temporal variability seen in many of the geochemical datasets from this and other studies within the Kura Basin. Initial uplift of the mountains due to regional compression, together with a relative sea level change, likely caused periods of increased restriction in the Kura Basin, resulting in the variable initial $^{187}Os/^{188}Os$ seawater values seen in the I-1 sample suite (Fig. 8). Furthermore, the unroofing and erosion of previously-deposited black shales as a result of uplift may have led to the release of previously-bound Os back into the basin. This may explain the anomalously high concentration of common Os in the Islamdag I-1 sample suite.

Complex variations in geochemical signals throughout the Kura Basin have been reported by many previous studies, and are reinforced by the Re-Os data, pyrolysis results and trace metal trends outlined here. Through adding qualitative and quantitative age control that places much of the studied stratigraphy in the Miocene, we propose that these trends are not only affected by regional tectonics related to the movement of the Arabian Plate, but within the Kura Basin they are also closely linked to orogenic activity along the Greater Caucasus and uplift during the Miocene.

CONCLUSIONS

A numerical age date for an anoxic event related to the isolation of the South Caspian region of the Paratethys has been obtained using Re-Os geochronology of the organic-rich Maikop Formation mudstones from sample sites in the Kura Basin, eastern Azerbaijan. The numerical age date produced for the lowest sampled interval of the Maikop Formation at Mount Islamdag places the time of deposition at 17.2 Ma. Intervals for which the geochronology was performed were analyzed for both bulk and trace elemental analysis to constrain depositional conditions, including geochemical indicators of anoxia, organic matter preservation, organic matter type and detrital input. The geochemical analyses

were also used to better constrain chemostratigraphic relationships of the Maikop using statistical cubic clustering analyses.

The results of previous studies indicate that the bulk of Maikop strata in the Kura Basin are not composed of deep-marine, anoxic black shales with high TOC; but are rather primarily composed of grey shales with a relatively low content of mainly terrigenous organic matter. New data from this study confirm these conclusions, and are consistent with infrequent development of anoxia during Maikop deposition and the preservation of organic matter in the Kura Basin. The only high TOC samples with marine organic matter came from the middle and lower parts of the succession at the Mount Islamdag location. The lower Islamdag sample suite was determined by Re-Os geochronology to have been deposited in the Burdigalian (~17.2 Ma), thereby providing a datum of reference for future stratigraphic correlation. This is the youngest age date yet to be produced by Re-Os geochronology on organic-rich mudstones, and displays the viability of this technique even on relatively young petroleum source rocks. Variable initial osmium ratios and the production of two geochronologically identical (within uncertainty) isochrons in the lower Islamdag sample suite are likely the result of rapid, dynamic basin shifts which are not however recorded in other observed geochemical indicators. High values of common Os in the Islamdag I-1 suite suggest an efficient mechanism of Os delivery related to the uplift and unroofing of the Greater Caucasus Mountains and the subsequent exposure and weathering of Os-rich materials. A more efficient uptake of Os into organic matter was due to the higher fraction of marine organic material found in the samples and the development of suboxic to anoxic bottom-water conditions, or a combination of these factors.

Where Re-Os geochronology was not definitive, qualitative age control of Maikopian strata was obtained by comparing 187Os/188Os values with the global 187Os/188Os sea level curve. The stratigraphically oldest strata studied, from just below what is commonly picked as the base of the Maikop Formation, was found to have been deposited near the Eocene – Oligocene Transition, as reflected by a significant 187Os/188Os excursion. This confirms the age proposed for the base of the Maikop Formation in the Kura Basin to around the Eocene – Oligocene Transition.

Comparisons of organic matter type and preservation, detrital input, indicators of anoxia, and correlation of the 187Os/188Os ratios with the global sea record showed that the basin was likely connected to the open ocean throughout much of the Miocene, but with important periods of restriction as the Kura and South Caspian Basins began to transition towards isolation. These periods of restriction are manifested by increased TOC, redox-sensitive major elements and trace metals, and initial Os excursions seen in sample suites from the Islamdag locality. The cause of suboxia/anoxia during these periods was likely related to increased restriction of the Kura Basin due to the uplift of the Greater Caucasus Mountains paired with regional tectonics related to the Arabian Plate impingement that finally isolated the entire Caspian Basin in the late Miocene. Increased detrital input may have resulted from variations in sediment supply due to the uplift of the Caucasus Mountains or to changes in sediment sources. Variations in the sediment source may also have influenced the influx and radiogenic nature of Re and Os brought into the system.

ACKNOWLEDGEMENTS

We would like to thank our friends at BP Azerbaijan for many years of collaboration in the Caspian region, and for the generous funding that made this research possible. We acknowledge the use of the laboratories at Brigham Young University and Durham University and the assistance of their staff, particularly Antonia Hoffmann at Durham, and Dave Tingey, Kevin Rey and Eric Christiansen at Brigham Young University. Preliminary reviews by Reinhard Sachsenhofer and David Boote are acknowledged, and we thank Christiaan van Baak for further detailed comments and suggestions which improved the paper significantly.

REFERENCES

ALGEO,T.J. and MAYNARD, J.B., 2004.Trace element behavior and redox facies in core shales of Upper Pennsylvanian Kansas-type cyclothems. Chem. Geol., 206, 289-318.

BAIOUMY, H.M., EGLINTON, L.B. and PEUKER-EHRENBRINK, B., 2011. Rhenium-osmium isotope and platinum group element systematics of marine vs. non-marine organic-rich sediments and coals from Egypt. Chem. Geol., 285, 70-81.

BECHTEL, A., MUVSUMOVA, U., PROSS, J., GRATZER, R., CORIC, S. and SACHSENHOFER, R. F., 2014. The Oligocene Maikop series of Lahich (eastern Azerbaijan): Paleoenvironment and oil-source rock correlation. Org. Geochem., 71, 43-59.

BRUNET, M.F., KOROTAEV, M.V., ERSHOV, A.V. and NIKISHKIN, A.M., 2003. The South Caspian Basin: a review of its evolution from subsidence modeling. Sedimentary Geology, 156, 119-148.

COHEN,A.S.,COE,A.L.,BARTLETT, J.M. and HAWKESWORTH, C.J ., 1999. Precise Re-Os ages of organic-rich mudrocks and the Os isotope composition of Jurassic seawater. Earth Planet. Sci. Lett., 167, 159-173.

COLODNER, D., SACHS., J., RAVIZZA, G., TUREKIAN, K.K., EDMOND, J. and BOYLE, E.A., 1993. The geochemical cycle of rhenium: a reconnaissance. Earth Planet. Sci. Lett., 117, 205-221.

CREASER, R.A., PAPANASTASSIOU, G. J. and WASSERBURG, G. J., 1991. Negative thermal ion mass spectrometry of osmium, rhenium, and iridium. Geochim. Cosmochim. Acta 55, 397-401.

CREASER, R.A., SANNIGRAHI, P., CHACKO,T. and SELBY, D., 2002. Further evaluation of the Re-Os geochronometer in organic-rich sedimentary rocks: A test of hydrocarbon maturation effects in Exshaw Formation, Western Canada Sedimentary Basin. Geochim. Cosmochim. Acta,66, 3341-3452.

CRUSIUS, J., CALVERT, S., PEDERSEN, T. and SAGE, D., 1996. Rhenium and molybdenum enrichments in sediments as indicators of oxic, suboxic, and sulfidic conditions of deposition. Earth Planet. Sci. Lett., 145, 65-78.

CUMMING, V. M., SELBY, D. and LILLIS, P.G., 2012. Re-Os geochronology of the lacustrine Green River Formation: Insights into direct depositional dating of lacustrine successions, Re-Os systematics and paleocontinental weathering. Earth Planet. Sci. Lett., 359-360, 194-205.

DALAI, T.K., RAVIZZA, G. and PEUCKER-EHRENBRINK, B., 2006. The Late Eocene 187Os/188Os excursion: Chemostratigraphy, cosmic dust flux and the early Oligocene glaciation. Earth Planet. Sci. Lett., 241, 477-492.

DICKIN, A.P., 2008. Radiogenic Isotope Geology. Cambridge University Press, Cambridge.

EFENDIYEVA, M., BABAEV, R., JOHNSON, C., FEYZULLAYEV, A. and ALIEV, C., 2012. Radiostratigraphic Study of the Deposits of the Maikop Group, Western Azerbaijan. Stratigraphy and Geological Correlation, 20, 567-577.

ERSHOV,A.V., BRUNET, M.F., NIKISHIN,A.M., BOLOTOV, S.N., NAZAREVICH, B.P., and KOROTAEV, M.V., 2003. Northern Caucasus basin: thermal history and synthesis of subsidence models. Sedimentary Geology, 156 (1-4), 95-118.

ESPITALIE, J., MADEC, M., TISSOT, B., MENNIG, J. J. and LEPLAT, P., 1977. Source rock characterization method for petroleum exploration. Offshore Technology Conference. doi: 10.4043/2935-MS

FERNEX, F., FÉVRIER, G., BENAÏM, J. and ARNOUX, A., 1992. Copper, lead and zinc trapping in Mediterranean deep-sea sediments: probable coprecipitation with manganese and iron. Chem. Geol. 98, 293-308.

GAETANI, M. and GARZANTI, E., 1991. Multicyclic history of the northern India continental margin (northwestern Himalaya). AAPG Bulletin, 75, 1427-1446.

GEORGIEV, S., STEIN, H.J., HANNAH, J.L., BINGEN, B.,WEISS, H.M. and PIASECKI, S., 2011. Hot acidic Late Permian seas stifle life in record time. Earth Planet. Sci. Lett., 310, 389- 400.

GEORGIEV, S., STEIN, H.J., HANNAH, J.L., WEISS, H.M., BINGEN, B., XU, G., REIN, E., HATLØ,V., LØSETH, H., NALI, M. and PIASECKI, S., 2012. Chemical signals for oxidative weathering predict Re-Os isochroneity in black shales, East Greenland. Chem. Geol., 324-325, 108-121.

GOLONKA, J., 2004. Plate tectonic evolution of the southern margin of Eurasia in the Mesozoic and Cenozoic. Tectonophysics, 381, 235-273.

HARRIS, N.B., MNICH, C.A., SELBY, D. and KORN, D., 2013. Minor and trace element and Re-Os chemistry of the Upper Devonian Woodford Shale, Permian Basin, west Texas: Insights into metal abundance and basin processes. Chem. Geol., 359, 76-93.

HUDSON, S.M., JOHNSON, C.L. and AFANDIYEVA, M.A., 2016. Spatial and temporal variability of Paleocene-Miocene organofacies of the Kura Basin, eastern Azerbaijan, and implications for basin evolution and petroleum generation. Org. Geochem., 97, 131-147.

HUDSON, S.M., JOHNSON, C.L., EFENDIYEVA, M.A., ROWE, H.D., FEYZULLAYEV, A.A. and ALIYEV, C.S., 2008. Stratigraphy and geochemical characterization of the Oligocene-Miocene Maikop series: implications for the paleogeography of Eastern Azerbaijan. Tectonophysics, 451, 40-55.

HUERTA-DIAZ, M.A. and MORSE, J. W., 1992. Pyritisation of trace metals in anoxic marine sediments. Geochim. Cosmochim. Acta, 56, 2681-2702.

INGAMELLS, C.O., 1970. Lithium metaborate flux in silicate analysis. Analytica Chimica Acta, 52, 323-334.

JOHNSON, C.L., HUDSON, S.M., ROWE, H.D., and EFENDIYEVA, M. A., 2010. Geochemical constraints on the Palaeocene-Miocene evolution of eastern Azerbaijan, with implications for the South Caspian Basin and eastern Paratethys. Basin Research, 22 (5), 733-750.

JONES, B. and MANNING, D. A., 1994. Comparison of geochemical indices used for the interpretation of palaeoredox conditions in ancient mudstones. Chemical Geology, 111(1-4), 111-129.

KAZ'MIN,V.G. and TIKHONOVA, N.F., 2006. Late Cretaceous- Eocene marginal seas in the Black Sea - Caspian Region: Paleotectonic reconstructions. Geotectonics, 40, 169-182.

KENDALL, B., CREASER, R.A. and SELBY, D., 2009. 187Re-187Os geochronology of Precambrian organic-rich sedimentary rocks. In: Global Neoproterozoic Petroleum Systems:The Emerging Potential in North Africa. Craig, J., Thurrow, J., Thusu, B., Whitham, A. and Abutarruma,Y., (Eds), Geol. Soc. London Special Publications, 326, 85-107.

KRYC, K.A., MURRAY, R.W. and MURRAY, D.W., 2003. Elemental fractionation of Si,Al,Ti, Fe, Ca, Mn, P, and Ba in five marine sedimentary reference materials: results from sequential extractions. Anal. Chim., 487, 117-128.

MIRSHAHANI, M., BAHRAMI, H., RASHIDI, M.,TARHANDEH, E. and KHANI, B., 2018. Organic geochemical evaluation of potential Cenozoic source rocks in the Moghan Basin, NW Iran: implications for hydrocarbon exploration. Journal of Petroleum Geology, 41(3), 393-410.

NAMEROFF, T.J., BALISTRIERI, L.S. and MURRAY, J.W., 2002. Suboxic trace metal geochemistry in the eastern tropical North Pacific. Geochim. Cosmochim. Acta, 66, 1139-1158.

NAMEROFF, T.J., CALVERT, S.E. and MURRAY, J.W., 2004. Glacial-interglacial variability in the eastern tropical North Pacific oxygen minimum zone recorded by redox- sensitive trace metals. Paleoceanography 19, PA 1010. doi:10.1029/2003PA000912.

NARIMANOV, A.A., 1993.The petroleum systems of the South Caspian Basin. In: DORÉ, A. G. et al. (Eds), Basin Modeling: Advances and Applications, 559-608.

PETERS, K. E. and CASSA, M.R. 1994. Applied source rock geochemistry: Chapter 5: Part II, Essential elements. In: Magoon, L. B. and Dow,W. G. (Eds),The Petroleum System - from source to trap. AAPG Memoir 60, 93-120.

PETERS, K.E., 1986. Guidelines for evaluating petroleum source rock using programmed pyrolysis. AAPG Bulletin, 3, 318-329.

PEUCKER-EHRENBRINK, B. and RAVIZZA, G., 2012. Osmium isotope stratigraphy. In: GRADSTEIN, F. M., OGG, J.G., SCHMITZ, M., and OGG, G. (Eds), The GeologicTime Scale. DOI: 10.1016/B978-0-444-59425-9.000008-1

PIPER, D.Z. and PERKINS, R.B., 2004. A modern vs. Permian black shale: hydrography, primary productivity and water- column chemistry of deposition. Chem. Geol. 206, 177-197.

POPOV, S.V. SYCHEVSKAYA, E.K., AKHMET'EV, M.A., ZAPOROZHETS, N.I., and GOLOVINA, L.A., 2008. Stratigraphy of the Maikop Group and pteropoda beds in Northern Azerbaijan. Strat. and Geol.Corr., 16, 664-677.

POPOV, S. V., VORONINA, A. A. and GONCHAROVA, I. A., 1993. Stratigraphy and bivalves of the Oligocene-Lower Miocene of the Eastern Paratethys. Inst. Ross.Akad. Nauk.

PUPP, M., BECHTEL,A., ĆORIC, S., GRATZER, R., RUSTAMOV, J. and SACHSENHOFER, R. F., 2018. Eocene and Oligo- Miocene Source Rocks in the Rioni and Kura Basins of Georgia: depositional environment and petroleum potential. Journal of Petroleum Geology, 41(3), 367-392.

RACIONERO-GOMEZ, B., SPROSON, A.D., SELBY, D., GANNOUN, A., GROCKE, D.R., GREENWELL, H.C., and BURTON, K.W., 2017. Osmium uptake, distribution and 187Os/188Os and 187Re/188Os compositions in Phaephyceae macroalgae, Fucus vesiculosus: implications for determining the 187Os/188Os composition of seawater. Geochim. Cosmochim. Acta, 199, 48-57.

RAVIZZA, G. and ESSER, B.K., 1993. A possible link between the seawater osmium isotope record and weathering of ancient sedimentary organic matter. Chem. Geol., 107, 255-258.

RAVIZZA, G. and TUREKIAN, K.K., 1989. Application of the 187Re-187Os system to black shale geochronometry. Geochim. Cosmochim. Acta, 53, 3257-3262.

RAVIZZA, G. and TUREKIAN, K.K., 1992.The osmium isotopic composition of organic-rich marine sediments. Earth and Planetary Science Letters, 110, 1-6.

RAVIZZA, G., TUREKIAN, K.K. and HAY, B.J., 1991. The geochemistry of rhenium and osmium in recent sediments from the Black Sea. Geochim. Cosmochim.Acta, 55, 3741-3752.

ROGL, F., 1999. Mediterranean and Paratethys - facts and hypotheses of an Oligocene to Miocene paleogeography (short overview). Geologica Carpathica, 50, 339-349.

ROONEY, A.D., CHEW, D.M. and SELBY, D., 2011. Re-Os geochronology of the Neoproterozoic-Cambrian Dalradian Supergroup of Scotland and Ireland: Implications for Neoproterozoic stratigraphy, glaciations and Re-Os systematics. Precambrian Research, 185, 202-214.

ROONEY, A.D., SELBY, D., HOUZAY, J. P.and RENNE, P.R., 2010. Re-Os geochronology of a Mesoproterozoic sedimentary succesion, Taoudeni basin, Mauritania: implications for basin- wide correlations and Re-Os organic-rich sediments systematics. Earth Planet. Sci. Lett., 289, 486-496.

ROONEY, A.D., SELBY, D., LEWAN, M.D., LILLIS, P.G. and HOUZAY, J.P., 2012. Evaluating Re-Os systematics in organic-rich sedimentary rocks in response to petroleum generation using hydrous pyrolysis experiments. Geochim. Cosmochim. Acta, 77, 275-291.

ROONEY, A.D., SELBY, D., LLOYD, J.M., ROBERTS, D.H., LÜCKGE, A., SAGEMAN,B.B. and PROUTY, N.G., 2016. Tracking millenial-scale Holocene glacial advance and retreat using osmium isotopes: Insights from the Greenland ice sheet. Quat. Sci. Reviews, 138, 49-61.

SACHSENHOFER, R. F., POPOV, S. V., CORIC, S., MAYER, J., MISCH, D., MORTON, M.T., PUPP, M., RAUBALL, J. andTARI, G., 2018. Paratethyan petroleum source rocks: an overview. Journal of Petroleum Geology, 41(3), 219-245.

SAINTOT, A., BRUNET, M.F., YAKOVLEV, F., SEBRIER, M., STEPHENSON, R., ERSHOV, A., CHALOT-PRAT, F., and McCANN, T., 2006. The Mesozoic-Cenozoic tectonic evolution of the Greater Caucasus. Geological Society, London, Memoir 32 (1), 277-289.

SELBY, D. and CREASER, R.A., 2003. Re-Os geochronology of organic rich sediments: an evaluation of organic matter analysis methods. Chem. Geol., 200, 225-240.

TRIBOVILLARD, N.,ALGEO,T.J., LYONS,T. and RIBOULLEAU, A., 2006.Trace metals as paleoredox and paleoproductivity proxies: an update. Chem. Geol., 232, 12-32.

VAN DER BOON, A., KUIPER, K.F., VILLA, G., RENEMA, W., MEIJERS, M.J.M., LANGEREIS, C.G., ALIYEVA, E. and KRIJGSMAN,W., 2015. Onset of Maikop sedimentation and cessation of Eocene arc volcanism in the Talysh Mountains, Azerbaijan. In: SOSSON, M., STEPHENSON, R.A. and ADAMIA, S.A. (Eds),Tectonic evolution of the Eastern Black Sea and Caucasus. Geol. Soc. London, Special Publications, 428, DOI: 10.1144/SP428.3

VINCENT, S. J., MORTON, A.C., CARTER, A., GIBBS, S., and BARABADZE,T.G., 2007. Oligocene uplift of the Western Greater Caucasus: an effect of initial Arabia–Eurasia collision. Terra Nova, 19, 160-166.

VOLKENING, J., WALCZYK, T. and HEUMANN, K.G., 1991. Osmium isotope ratio determinations by negative thermal ionization mass spectrometry. International Journal of Mass Spectrometry and Ion Processes, 105 (2), 147-159.

WASHBURN,A.M., HUDSON, S.M., SELBY, D.,ABDULLAYEV, N. and SHIYANOVA, N., 2018. Re-Os geochronology and chemostratigraphy of the Maikop Series source rocks of eastern Azerbaijan [Extended Abstract]. Journal of Petroleum Geology, 41 (3), 411-416.

WEDEPOHL, K. H., 1991.The composition of the upper Earth's crust and the natural cycles of selected metals. Metals in natural raw materials. Natural Resources. In: Merian, E. (Ed.), Metals and Their Compounds in the Environment. VCH,Weinheim, 3-17.

WEDEPOHL, K.H., 1971. Environmental influences on the chemical composition of shales and clays. Phys. and Chem. of the Earth, 8, 307-333.

WILKS, D. S., 2011. Cluster analysis. International Geophysics, 100, 603-616. Academic Press.

WOOD, S.A. and SAMSON, I.M., 2006. The aqueous geochemistry of gallium, germanium, indium and scandium. Ore Geology Reviews, 28, 57-102.

YAMASHITA,Y.,TAKAHASHI,Y., HABA, H., ENOMOTO, S. and SHIMIZU, H., 2007. Comparison of reductive accumulation of Re and Os in seawater-sediment systems. Geochim. Cosmochim. Acta, 71, 3485-3475.

Table 1. Summary of pyrolysis data, showing mean, minimum and maximum values for each sample suite. All the data were obtained using a HAWK pyrolysis analyser.

Sample Suite	Value	S1-Free Oil (mgHC/g rock)	S2-Kerogen Yield (mgHC/g rock)	S3 (mgCO2/g rock)	Tmax-Maturity (°C)	TOC-Total Organic Carbon (Weight %)	CC-Carbonate Carbon (Weight %)	GOC-Generative OC (Weight %)	NGOC-Non-generative OC (Weight %)	AI-Adsorption Index (Weight %)	OSI-Oil Sat.Index (mgHC/gTOC)	PI-Production Index	HI-Hydrogen Index (mgHC/gTOC)	OI-Oxygen Index (mgCO2/gTOC)
Islamdag	Average	0.33	8.22	0.56	421.80	2.29	0.13	0.77	1.53	1.88	11.36	0.07	265.48	39.44
	Min	0.03	0.15	0.27	402.00	0.58	0.10	0.04	0.53	0.48	3.00	0.03	24.00	11.00
	Max	1.00	28.44	0.96	434.00	4.58	0.22	2.55	2.89	3.76	21.00	0.29	620.00	125.00
I-3	Average	0.04	0.22	0.57	431.88	0.68	0.13	0.05	0.63	0.56	5.13	0.15	31.88	84.38
	Min	0.03	0.15	0.37	430.00	0.58	0.10	0.04	0.53	0.48	3.00	0.10	24.00	58.00
	Max	0.08	0.31	0.76	434.00	0.83	0.17	0.06	0.78	0.68	12.00	0.29	41.00	125.00
I-2	Average	0.56	15.47	0.45	427.33	2.99	0.12	1.40	1.59	2.46	17.44	0.04	481.33	15.89
	Min	0.23	4.70	0.27	425.00	1.47	0.10	0.45	1.02	1.21	15.00	0.03	319.00	11.00
	Max	1.00	28.44	0.60	431.00	4.58	0.16	2.55	2.04	3.76	21.00	0.05	620.00	32.00
I-1	Average	0.35	8.06	0.68	405.50	3.12	0.14	0.77	2.35	2.56	10.75	0.04	256.25	21.00
	Min	0.28	6.19	0.52	402.00	2.67	0.11	0.60	2.05	2.19	10.00	0.04	231.00	17.00
	Max	0.50	10.38	0.96	408.00	3.82	0.22	1.00	2.89	3.14	13.00	0.05	299.00	25.00
Perikeshkul	Average	0.04	0.14	0.72	378.47	0.64	1.64	0.05	0.59	0.52	6.63	0.35	17.68	153.05
	Min	0.01	0.01	0.24	341.00	0.18	0.07	0.02	0.16	0.15	1.00	0.12	3.00	36.00
	Max	0.09	0.51	1.23	424.00	2.45	8.27	0.10	2.36	2.01	14.00	0.57	47.00	271.00
P-3	Average	0.09	1.05	0.77	429.75	1.28	0.10	0.14	1.14	1.05	6.75	0.08	80.50	60.25
	Min	0.06	0.68	0.60	428.00	0.99	0.06	0.09	0.89	0.81	6.00	0.07	61.00	49.00
	Max	0.12	1.50	0.86	431.00	1.49	0.17	0.17	1.31	1.22	8.00	0.10	100.00	69.00
P-2	Average	0.01	0.01	0.35	359.60	0.21	0.10	0.03	0.19	0.18	5.20	0.47	6.40	165.00
	Min	0.01	0.01	0.24	344.00	0.18	0.07	0.02	0.16	0.15	4.00	0.37	5.00	134.00
	Max	0.01	0.02	0.43	397.00	0.25	0.12	0.03	0.22	0.21	6.00	0.53	11.00	221.00
P-1	Average	0.07	0.29	1.05	393.67	0.90	1.80	0.07	0.83	0.74	8.56	0.23	31.00	151.44
	Min	0.05	0.10	0.87	366.00	0.36	0.83	0.05	0.31	0.30	3.00	0.12	20.00	41.00
	Max	0.09	0.51	1.23	419.00	2.45	2.29	0.10	2.36	2.01	14.00	0.35	47.00	264.00
Shikhzahirli	Average	0.08	1.80	0.47	421.00	0.99	0.40	0.19	0.80	0.81	7.71	0.06	164.00	51.75
	Min	0.03	0.22	0.27	413.00	0.39	0.07	0.05	0.35	0.32	4.00	0.03	54.00	24.00
	Max	0.14	3.24	0.79	429.00	1.39	0.89	0.32	1.09	1.14	12.00	0.12	248.00	113.00
S-3	Average	0.04	0.71	0.50	421.25	0.67	0.37	0.09	0.57	0.55	5.88	0.07	101.38	77.13
	Min	0.03	0.22	0.36	417.00	0.39	0.24	0.05	0.35	0.32	4.00	0.03	54.00	52.00
	Max	0.06	1.69	0.63	424.00	0.89	0.57	0.18	0.74	0.73	7.00	0.12	189.00	113.00
S-2	Average	0.10	1.78	0.38	414.88	1.02	0.12	0.19	0.83	0.84	9.88	0.07	163.25	38.13
	Min	0.08	0.73	0.27	413.00	0.75	0.07	0.10	0.66	0.62	7.00	0.04	97.00	29.00
	Max	0.14	3.09	0.52	417.00	1.39	0.15	0.31	1.09	1.14	12.00	0.10	235.00	51.00
S-1	Average	0.10	2.92	0.52	426.88	1.28	0.72	0.29	0.99	1.05	7.38	0.03	227.38	40.00
	Min	0.09	2.58	0.32	425.00	1.23	0.53	0.26	0.95	1.01	7.00	0.03	194.00	24.00
	Max	0.11	3.24	0.79	429.00	1.33	0.89	0.32	1.07	1.09	8.00	0.04	248.00	62.00

Table 2. Summary of geochemical data used to interpret detrital and anoxic conditions in the sample suites. All data presented are average values, and were measured using ICP-OES unless otherwise noted. Values for average shale obtained from Wedepohl *et al.*, 1971; 1991.

	Al	Cr	Cu	Ga (XRF)	La (XRF)	Mo	Ni	Sc (XRF)	Ti	Th (XRF)	U (XRF)	V
Average Shale	167000	90	45	19	40	1.3	68	13	7800	-	3.7	130
I-1	13058.95	125.74	99.64	20.45	29.84	77.60	179.11	14.65	7771	11.96	28.25	342.40
I-2	14078.77	117.64	116.85	17.47	24.57	10.44	123.65	11.88	6292	9.36	3.48	144.10
I-3	11973.27	155.69	65.41	26.01	38.85	7.68	79.93	20.15	8820	13.60	4.31	178.59
P-1	16054.54	32.26	33.28	12.94	17.30	6.46	29.64	6.10	5335	13.28	2.92	43.76
P-2	15752.86	134.30	25.72	14.13	16.62	6.11	34.30	12.49	4762	13.11	2.55	106.38
P-3	18007.47	152.05	87.13	25.64	36.59	8.47	91.91	19.55	7984	12.83	4.25	178.19
S-1	11918.22	107.71	62.77	18.50	32.77	13.25	60.12	14.39	7466	11.84	4.46	143.99
S-2	16474.29	99.38	48.03	18.24	31.69	9.00	87.21	11.79	7033	11.35	4.21	122.15
S-3	17165.67	80.71	30.16	11.41	27.33	13.88	47.05	7.16	6507	9.05	4.29	74.70

Table 3. Full data set for measured Re-Os isotopes in each sample, with average values at the base of each sample suite. All initial osmium isotope values were calculated at 17.2 Ma.

Batch/Sample	Re (ppb)	±	Os (ppt)	±	192Os (ppt)	±	187Re/188Os	±	187Os/188Os	±	rho	% Re Blank	% 187Os Blank	% 188Os Blank	Osi @ XX myr	±
I-1 (1)	314.5	0.8	585.2	2.7	200.7	0.7	3117.1	13.7	1.689	0.009	0.579	0.013	0.010	0.067	0.80	0.01
I-1 (2)	376.4	0.9	489.3	2.3	163.4	0.6	4583.6	19.6	1.940	0.010	0.581	0.011	0.010	0.082	0.63	0.02
I-1 (3)	421.7	1.0	453.9	2.3	144.2	0.5	5817.4	25.8	2.423	0.012	0.589	0.009	0.010	0.093	0.76	0.02
I-1 (4)	412.6	1.0	598.8	2.7	202.7	0.7	4048.5	17.3	1.809	0.009	0.577	0.010	0.009	0.066	0.65	0.01
I-1 (5)	111.3	0.3	300.8	1.3	106.9	0.4	2070.6	9.2	1.365	0.007	0.601	0.036	0.023	0.125	0.77	0.01
I-1 (6)	167.2	0.4	437.9	1.7	158.5	0.6	2098.8	9.0	1.205	0.006	0.585	0.024	0.017	0.084	0.60	0.01
I-1 (7)	413.9	1.0	442.9	2.2	141.8	0.5	5806.5	25.2	2.345	0.012	0.583	0.010	0.010	0.094	0.68	0.02
I-1 (8)	313.1	0.8	450.7	2.2	149.7	0.6	4161.1	18.6	1.992	0.011	0.567	0.013	0.011	0.089	0.80	0.02
Average	316.3		469.9		158.5		3963.0		1.846		0.583	0.016	0.013	0.088	0.710	
S-1 (1)	14.34	0.04	134.5	0.5	49.9	0.2	572.3	2.8	0.998	0.006	0.630	0.03	0.04	0.16	0.83	0.01
S-1 (2)	13.19	0.03	137.2	0.6	51.0	0.2	514.8	2.5	0.983	0.006	0.621	0.04	0.04	0.16	0.84	0.01
S-1 (3)	15.79	0.04	136.4	0.6	50.5	0.2	621.8	3.0	1.003	0.006	0.626	0.03	0.04	0.16	0.83	0.01
S-1 (4)	15.99	0.04	136.7	0.6	50.7	0.2	627.9	3.1	0.998	0.006	0.616	0.03	0.04	0.16	0.82	0.01
S-1 (5)	14.99	0.04	138.1	0.6	51.2	0.2	582.8	2.8	0.999	0.006	0.625	0.03	0.04	0.16	0.83	0.01
S-1 (6)	17.55	0.04	138.6	0.6	51.4	0.2	679.2	3.3	0.994	0.006	0.624	0.03	0.04	0.16	0.80	0.01
S-1 (7)	15.12	0.04	130.8	0.6	48.5	0.2	620.3	3.3	0.999	0.007	0.645	0.03	0.04	0.17	0.82	0.01
S-1 (8)	13.49	0.03	172.3	0.6	65.6	0.3	408.9	1.9	0.767	0.004	0.610	0.04	0.04	0.12	0.65	0.00
Average	15.06		140.56		52.34		578.51		0.968		0.625	0.032	0.040	0.155	0.802	
P-3 (1)	2.27	0.01	199.5	1.2	75.5	0.7	59.9	0.6	0.821	0.010	0.667	0.53	0.02	0.05	0.80	0.01
P-3 (2)	2.01	0.01	176.9	1.1	67.3	0.6	59.3	0.5	0.783	0.010	0.677	0.60	0.02	0.06	0.77	0.01
P-3 (3)	1.48	0.00	150.3	0.9	57.2	0.5	51.6	0.5	0.778	0.010	0.673	0.81	0.02	0.07	0.76	0.01
P-3 (4)	1.50	0.00	156.1	0.9	59.5	0.5	50.0	0.5	0.771	0.009	0.674	0.80	0.02	0.07	0.76	0.01
P-3 (5)	2.54	0.01	202.0	1.2	76.9	0.7	65.8	0.6	0.774	0.010	0.678	0.47	0.02	0.05	0.76	0.01
P-3 (6)	1.98	0.01	169.3	1.0	64.4	0.6	61.2	0.6	0.779	0.010	0.675	0.61	0.02	0.06	0.76	0.01
P-3 (7)	1.63	0.00	165.3	1.0	63.1	0.6	51.5	0.5	0.752	0.009	0.674	0.74	0.02	0.06	0.74	0.01
P-3 (8)	2.36	0.01	227.0	1.3	88.7	0.8	52.9	0.5	0.561	0.007	0.678	0.51	0.02	0.05	0.55	0.01
Average	1.97		180.80		69.07		56.52		0.75		0.67	0.63	0.02	0.06	0.74	
I-3 (1)	1.08	0.00	146.21	0.98	56.1	0.6	38.4	0.4	0.708	0.011	0.674	1.11	0.02	0.07	0.70	0.01
I-3 (2)	1.33	0.01	165.71	1.13	64.0	0.7	41.3	0.6	0.654	0.011	0.475	0.90	0.02	0.06	0.64	0.01
I-3 (3)	1.12	0.00	125.07	0.85	48.0	0.5	46.5	0.5	0.709	0.011	0.676	1.07	0.03	0.08	0.70	0.01
I-3 (4)	1.31	0.00	130.92	0.71	50.1	0.4	51.9	0.4	0.734	0.008	0.650	0.92	0.02	0.08	0.72	0.01
I-3 (5)	1.47	0.00	152.00	0.78	58.8	0.4	49.8	0.4	0.649	0.007	0.658	0.82	0.02	0.07	0.63	0.01
I-3 (6)	1.22	0.00	146.84	0.77	56.2	0.4	43.2	0.3	0.725	0.008	0.656	0.98	0.02	0.07	0.71	0.01
I-3 (7)	1.04	0.00	280.48	1.24	112.1	0.8	18.5	0.1	0.377	0.004	0.648	1.15	0.02	0.04	0.37	0.00
I-3 (8)	0.95	0.00	116.75	0.62	44.8	0.3	42.1	0.3	0.718	0.008	0.640	1.27	0.03	0.09	0.71	0.01
Average	1.19		158.00		61.26		41.45		0.66		0.63	1.03	0.02	0.07	0.65	
P-1 (1)	5.71	0.01	213.15	0.61	84.4	0.3	134.5	0.6	0.456	0.002	0.581	0.21	0.02	0.05	0.42	0.00
P-1 (2)	10.63	0.03	276.93	0.83	109.6	0.4	192.9	0.9	0.459	0.003	0.594	0.11	0.02	0.04	0.40	0.00
P-1 (3)	9.85	0.02	518.20	1.46	209.0	0.9	93.8	0.5	0.310	0.002	0.600	0.12	0.01	0.02	0.28	0.00
P-1 (4)	8.37	0.02	275.89	0.90	108.9	0.5	152.9	0.8	0.478	0.003	0.608	0.14	0.02	0.04	0.44	0.00
P-1 (5)	6.45	0.02	259.83	0.95	103.0	0.5	124.5	0.7	0.445	0.003	0.636	0.19	0.02	0.04	0.41	0.00
P-1 (6)	19.30	0.05	267.91	0.76	106.1	0.4	361.8	1.6	0.450	0.002	0.577	0.06	0.02	0.04	0.35	0.00
P-1 (7)	13.19	0.03	324.43	0.99	128.5	0.5	204.2	1.0	0.450	0.003	0.594	0.09	0.02	0.03	0.39	0.00
P-1 (8)	6.17	0.02	196.90	0.73	77.9	0.4	157.7	0.9	0.464	0.003	0.638	0.19	0.02	0.05	0.42	0.00
Average	9.96		291.65		115.92		177.81		0.44		0.60	0.14	0.02	0.04	0.39	